

# We are IntechOpen, the world's leading publisher of Open Access books Built by scientists, for scientists

6,900

Open access books available

186,000

International authors and editors

200M

Downloads

Our authors are among the

154

Countries delivered to

TOP 1%

most cited scientists

12.2%

Contributors from top 500 universities



WEB OF SCIENCE™

Selection of our books indexed in the Book Citation Index  
in Web of Science™ Core Collection (BKCI)

Interested in publishing with us?  
Contact [book.department@intechopen.com](mailto:book.department@intechopen.com)

Numbers displayed above are based on latest data collected.  
For more information visit [www.intechopen.com](http://www.intechopen.com)



## Fe-Al Alloys' Magnetism

F. Plazaola<sup>1</sup>, E. Apiñaniz<sup>3</sup>, D. Martin Rodriguez<sup>4</sup>,  
E. Legarra<sup>1</sup> and J. S. Garitaonandia<sup>2</sup>

<sup>1</sup>*Elektrika eta Elektronika Saila, Euskal Herriko Unibertsitatea UPV/EHU, Bilbao,*

<sup>2</sup>*Fisika Aplikatua II Saila, Euskal Herriko Unibertsitatea UPV/EHU, Bilbao,*

<sup>3</sup>*Fisika Aplikatua I Saila, Euskal Herriko Unibertsitatea UPV/EHU, Bilbao,*

<sup>4</sup>*Jülich Centre for Neutron Science and Institute for Complex Systems,*

*Forschungszentrum Jülich GmbH, Jülich,*

<sup>1,2,3</sup>*Spain*

<sup>4</sup>*Germany*

### 1. Introduction

Intermetallic compounds and ordered intermetallic structures have attracted great interest for both scientific reasons and their possible technological applications [1, 2]. These materials are widely used as high temperature structural materials, functional materials for scientific applications, as diffusion barriers, and as contacts and interconnections in microelectronics.

In this chapter we will study the magnetism of Fe-Al intermetallic alloys. Interest in these alloys grew after 1930 when their excellent oxidation resistance was discovered. Iron aluminides are intermetallics, which apart from the good oxidation resistance offer excellent sulphidation resistance and potentially lower cost compared to many other high temperature materials. Additionally, they have densities that are about 30 % lower than commercial high temperature structural materials, such as stainless steel or Ni based superalloys. It has also been found that Fe-Al alloys with different magnetic and physical properties can be obtained by varying the composition and their heat treatments [3]. However, the limited ductility at room temperature and the decrease in strength above 600 °C are still drawbacks that limit their exploitation for structural applications.

The mechanical and magnetic properties of the Fe-Al intermetallic alloys strongly depend on the deviation from the stoichiometry, and the addition of a ternary alloy component can improve the ductility at room temperature and the strength at high temperature.

All the properties mentioned make these alloys of great technological importance; that is the reason why they have been widely studied for the last decades. In addition, many first principle investigations on the electronic and magnetic structure have been conducted to provide a microscopic understanding of the chemical bonding, the formation of clusters, the surfaces and the phase stability.

As far as magnetism is concerned, one of the most prominent features of Fe-rich Fe-Al alloys is that any structural change is directly reflected by their magnetic behavior. That is to say, any slight mechanical deformation produced on the ordered alloy causes an abrupt increase of the ferromagnetic signal [4-12]; in fact, this alloy presents an unusual ease to undergo order-disorder transitions. Indeed, with a simple crushing, a solid solution structure is induced and the cell parameter can increase by even as much as 1% in some of the alloys. This change is reflected immediately by the magnetic behavior of the material. For instance, for certain compositions ordered samples present a great paramagnetic contribution, but they become strongly ferromagnetic when crushed. Moreover, small changes in Fe content of the alloy (less than 1 at. %) induce large changes in its magnetic behavior [13, 14]. In order to explain these behaviors the intimate relationship between microstructure and magnetism has to be taken into account; indeed, this is linked to the fact that the iron rich side of FeAl phase diagram (see fig. 1) presents three main phases: ordered D03 and B2, and disordered A2. For this reason, Fe-rich FeAl intermetallic alloys are considered as a "test field" to test theories and hypothesis of fundamental magnetism. Figure 2 shows the three structures mentioned before. A2 structure is a solid solution, and therefore the Fe and Al atoms are distributed at random in the crystallographic positions of a bcc structure. B2 structure is a CsCl type structure, with a stoichiometric composition of  $\text{Fe}_{50}\text{Al}_{50}$ , where the Fe atoms site is the vertex (position A) and Al atoms sit in the center (position B) of the cube. The D03 structure consists of four interpenetrating face centered cubic sublattices. For the stoichiometric composition ( $\text{Fe}_{75}\text{Al}_{25}$ ) Fe atoms occupy A, B and C non-equivalent positions and Al atoms occupy D positions.

Apart from the properties mentioned above, these alloys show an important effect that it is worth mentioning: magnetostriction, i.e. change of the sample dimensions in response to an applied field. This property makes Fe-Al alloys interesting because of their potential use as low-cost sensor devices. Room temperature magnetostriction measurements of Fe-Al alloys indicated a five-fold rise in magnetostriction with Al additions up to 30% Al [16, 17]. These works, performed on single crystals, concluded that there was a large temperature dependence of the magnetostriction of the materials and they added that the stabilization of the disordered bcc structure was a fundamental component in the increase of the magnetostriction of the materials. On the other hand, higher magnetostriction values were found for rapidly quenched ribbons [18, 19, 20] and the microstructure and the room-temperature magnetostriction of polycrystalline FeAl alloys have also been studied [21]. These last works conclude that the magnetostriction of this system is very dependent on the heat treatment (and therefore, the structure), the temperature and the composition.

Another important magnetic property that will be studied in this chapter is the spin-glass and re-entrant spin-glass (or mictomagnetism) phenomena found at low temperatures for certain alloys. One of the direct consequences is the anomalous magnetization-increase that the magnetization curves show at low temperatures with the increase of the temperature [5, 22], in a certain range of Fe concentrations. Spin-glass systems are characterized by an absence of magnetic order below the denominated freezing temperature ( $T_f$ ) as a consequence of weakening of magnetic exchange mechanisms among magnetic moments.

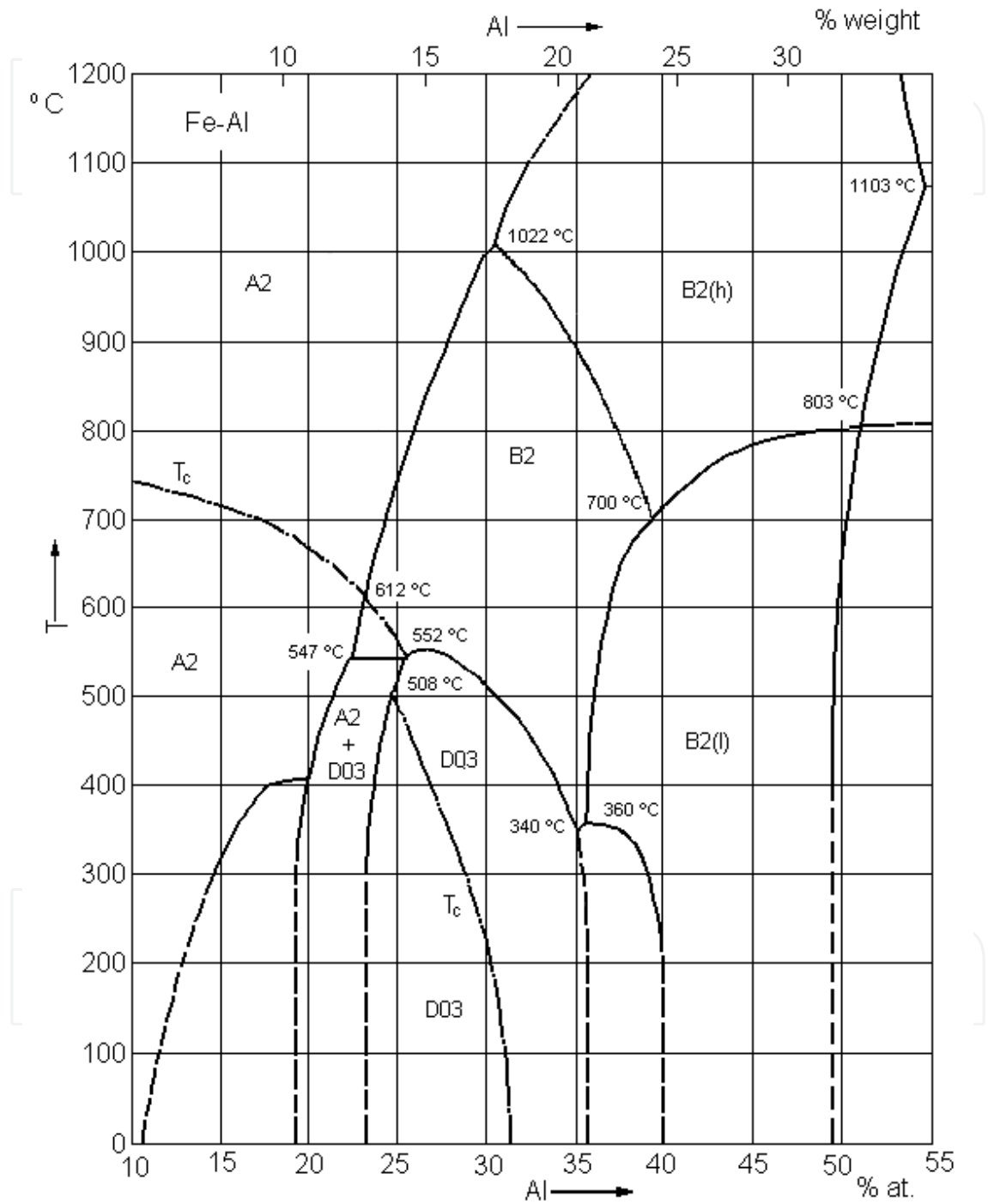


Fig. 1. Phase diagram of the Fe rich side Fe-Al system [15].

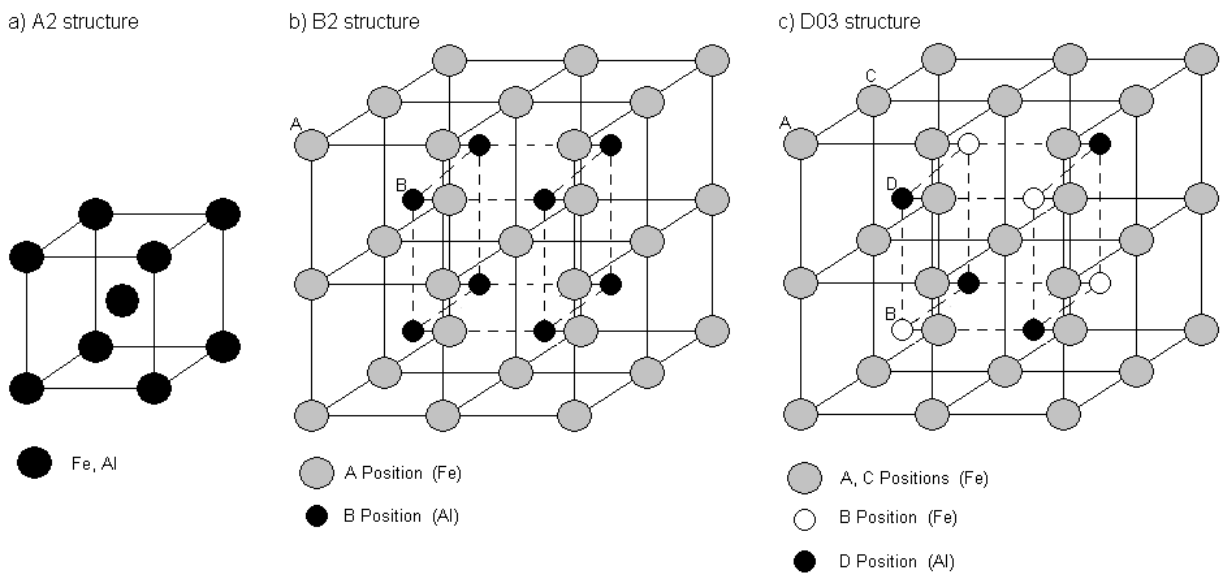


Fig. 2. Main crystallographic structures of the Fe rich side phase diagram: a) disordered A2 structure, b) B2 structure and c) D03 structure.

The Fe-Al system has a 3d transition element. It is widely known that one of the most important topics of magnetism is the study of the magnetic interactions between 3d magnetic elements and the magnetic effects and properties presented in the magnetic materials that they form. There are two main reasons that make this topic very important: On the one hand, the 3d based magnetic materials are used in many industrial applications; any study that can help in understanding the origin of the magnetic properties of this kind of materials could be used to improve them or to produce materials adapted or optimized for each application. On the other hand, these kinds of studies are fundamental from the point of view of basic magnetism. Most of the theories that try to explain the physical mechanism of the magnetic exchange interactions between 3d elements are qualitative. Usually the source of these theories is the Bethe-Slater curve [23], which explains the different magnetic behaviors of the materials in terms of differences in the exchange interactions between the magnetic elements. The verification of this curve and the theory hidden behind is one of the main aims in the field of magnetism. Fe-Al alloys are suitable to study the role of the structure on the magnetism of the materials, because they represent a simple model with well known ordered structures for studying the basic properties. In addition, it also presents a wide variety of magnetic behaviors as mentioned above (ferromagnetic, paramagnetic, spin-glass, re-entrant spin-glass), which is a clue to the existence of different kinds of exchange interactions in this alloy system.

The origin of magnetism of these alloys has been investigated by different techniques, as will be shown in the following sections. We have divided the experimental study of the magnetism of Fe-Al alloys in three subsections. In the first one the unusual magnetic properties of the ordered alloys are described. In the next one the contributions to the magnetic signal increase with disorder and the disordering process are presented and in the last one the reordering process is discussed. It has to be mentioned that the most complex magnetism in FeAl binary alloys is around Fe<sub>70</sub>Al<sub>30</sub> composition; therefore, in this chapter we will pay plenty of attention to such a composition.

Finally, we will end up our work by showing the results of theoretical calculations performed for FeAl alloys for different structures and compositions.

## 2. Ordered alloys

FeAl alloys are a well-suited system for the study of the properties of magnetic materials and in particular, for study of the role of the structure on the magnetic character of those materials [4, 6, 8, 10, 24-26]. Due to the existence of only one magnetic atom and the structural simplicity of a binary system, the theoretical results can be easily related to the magnetic properties [27-30].

The room temperature magnetic moment of ordered iron aluminides (Fe<sub>1-x</sub>Al<sub>x</sub>) decreases slowly with increasing Al content up to  $x=0.2$ , which is consistent with dilution models. With further dilution the magnetic moment decreases more rapidly, becoming zero for alloys with  $x \geq 0.325$  of Al [31]. Martin Rodriguez et al. [32] and Schmool et al. [33] showed by Mössbauer spectra measured at room temperature how the ferromagnetic network breaks into magnetic clusters with the addition of Al at room temperature above  $x=0.275$  and the magnetic hyperfine field becomes zero at room temperature for  $x \geq 0.325$ . X-ray diffraction patterns show traces of D03 structured domains for  $x < 0.325$ . However, for  $0.325 \leq x \leq 0.5$  the ordered alloys present only B2 structure, showing evidences that both, a magnetic transition and a structural transition, occur around  $x=0.325$  at RT, which suggests a strong correlation between the intermetallic order and the magnetic behavior in this alloy system [32].

According to the molecular field model, saturation magnetization is expected to decrease with increasing temperature. In contrast, in Fe-Al alloys the opposite tendency has been observed in samples with Al concentration in the range  $0.275 < x < 0.325$ . In this section we will focus on discussing that unusual increase of the magnetic signal that occurs for samples with about 68-72 at.% Fe content. Figure 3 shows some selected M(H) curves obtained at several temperatures, for the Fe<sub>70</sub>Al<sub>30</sub> ordered sample. Although the magnetization increase rate depends strongly on the applied field, figure 3 indicates that the maximum increase of the magnetization curve is located somewhere between 150 K and 200 K. Arrott and Sato [5, 34] observed this effect in 1959 for the first time. The structural characterization published two years before [4] showed that the structure of the Fe<sub>70</sub>Al<sub>30</sub> ordered sample was Fe<sub>3</sub>Al type (D03 structure). Based on that crystallographic structure and on the evolution with temperature of the hysteresis curves, the authors proposed a model where nearest-neighbors Fe-Fe ferromagnetic exchange competed with indirect Fe-Al-Fe antiferromagnetic super-exchange. However, later neutron diffraction results [35] proved that, below the Curie temperature, the alloy always presented a ferromagnetic character, and the model was abandoned. Since those results, several papers have been published, suggesting the

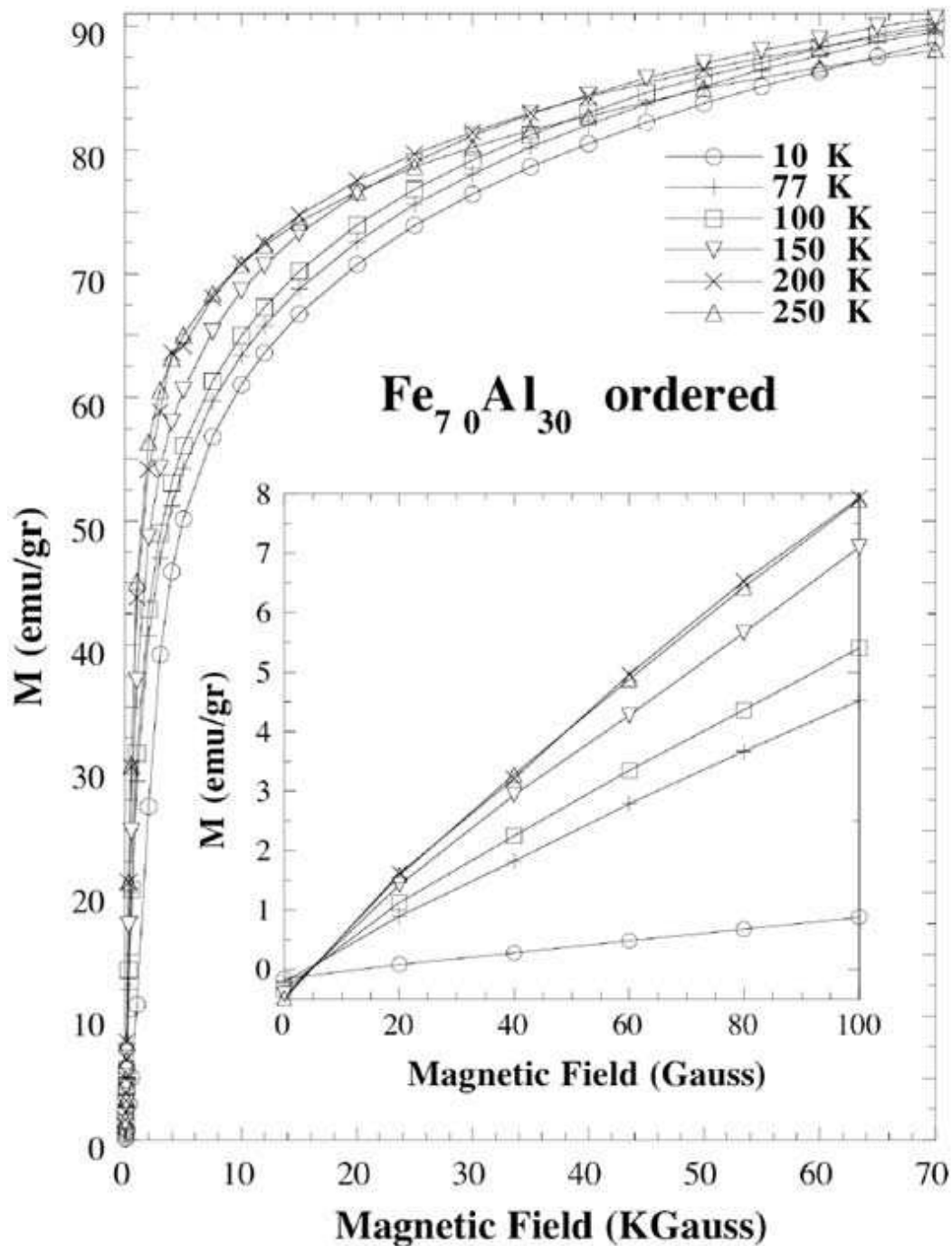


Fig. 3. Magnetization curves,  $M(H)$ , of the  $\text{Fe}_{70}\text{Al}_{30}$  alloy obtained at different temperatures. Before measuring every  $M(H)$  curve the sample was demagnetized. The inset shows the detail of the  $M(H)$  curves for applied fields below 0.01 T.

existence of a phenomenon known as mictomagnetism [10, 36, 37]. The mictomagnetism consisted in a collective freezing of the spin re-orientations at certain temperatures without long magnetic order. In the case of the FeAl alloys, this last fact implied that the behavior of the magnetism was local. Nowadays, we know that almost all mictomagnetic processes are associated with spin-glass or reentrant spin-glass processes. The transition to a spin-glass state is clearly detected by a comparison of the evolution of the magnetic signal with the

temperature when the system has been zero-field-cooled (ZFC) and field-cooled (FC) from a paramagnetic regime. In the first case the material is cooled without applied field from temperatures higher than the Curie one ( $T_c$ ), which makes the moments keep their random orientations at lower temperatures. The ZFC curve is obtained starting from such a situation, applying a small external field while increasing the temperature, which adds energy to the system and allows the magnetic moments to start orientating gradually into the direction of the applied field. However, in the FC case the system is cooled under an external magnetic field, which aligns the moments in the direction of the applied field once the temperature decreases below  $T_c$ . The difference in the initial state (moments already oriented or disoriented) is reflected in the different behaviors with the temperature of the ZFC-FC curves up to the freezing temperature ( $T_f$ ), when the magnetic exchange among moments is strong enough to establish a long range order and to maintain intrinsically the moments oriented.

As it can be observed in Figure 4,  $\text{Fe}_{70}\text{Al}_{30}$  ordered sample enters in a spin-glass like regime below  $T_f \sim 90$  K. This transition is also consequence of the predominance of the local mechanisms governing the magnetism of this alloy.

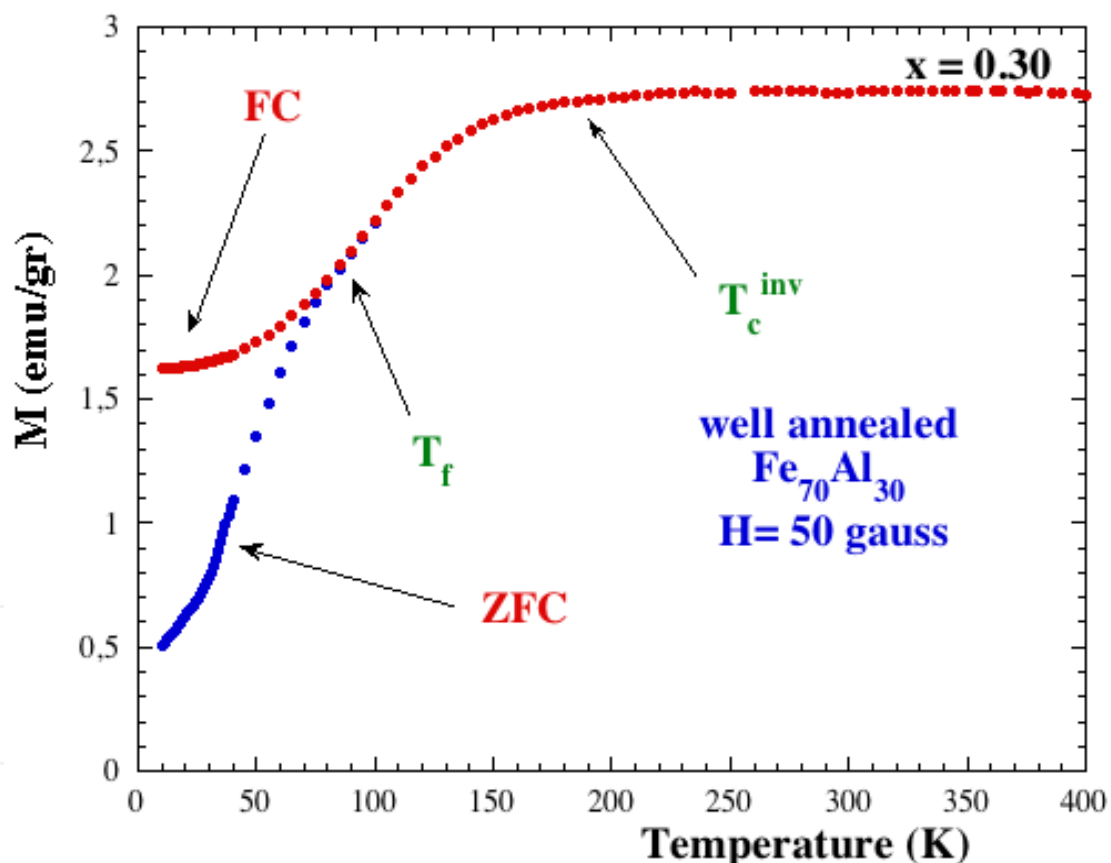


Fig. 4. ZFC and FC curves of the  $\text{Fe}_{70}\text{Al}_{30}$  alloy. The FC curve was obtained under an applied field of 50 gauss.  $T_c^{\text{inv}}$  and  $T_f$  are transition temperatures (see text).

Figure 4 shows the ZFC-FC magnetization curves obtained at 50 gauss applied field for the studied sample. The  $T_f$  and  $T_c^{\text{inv}}$  temperatures indicate magnetic transition points. The transition points represent the limits of three different zones. The first zone ranges from the lowest temperatures up to  $T_f \sim 90$  K. This zone is concerned with different evolutions of magnetization with temperature for field cooled or zero field cooled samples. In the second

zone, which ranges from  $T_f$  temperature up to  $T_c^{inv}$  labeled temperature ( $\sim 180$  K), the magnetization increases with temperature. In the last zone (from  $T_c^{inv}$  temperature up) the magnetic signal remains constant.

Other peculiarity of the magnetization curves (figure 3) is the pronounced slope they present in the high field zone. The signal does not reach saturation even at 70 kgauss applied field. This fact is a clear indication of the existence of paramagnetic type behavior in the sample. Magnetic neutron scattering results as well as detailed magnetic measurements showed that the mictomagnetism is accompanied by a superparamagnetic character of FeAl alloys [37-40]. The superparamagnetism is the consequence of complex magnetic structure, composed by dynamical ferromagnetic clusters accommodated in a paramagnetic crystalline matrix. The discussion is centered on the evolution with temperature of the paramagnetic contribution, and on its role in the magnetic interaction among clusters [38, 41-43]. The magnetic picture of the  $Fe_{70}Al_{30}$  ordered sample is the result of the coexistence of two different magnetic phases that follow different behaviors with temperature and, so, with different magnetic relations between them.

Mössbauer spectroscopy is a very useful technique for studying the electronic structure of solids such as chemical bonding or magnetism as it allows the detection of variations in the nuclear energy levels due to the electromagnetic coupling between nuclear and electronic charges. These variations are known as hyperfine interactions and they may shift energy levels or lift their degeneracy. In the presence of a magnetic field the interaction between the nuclear spin moments with the magnetic field removes all the degeneracy of the energy levels resulting in the splitting of energy levels. For iron atoms this magnetic splitting will result in a sextet. Thus, Mössbauer spectroscopy is able to distinguish magnetic and non-magnetic phases. For cubic structures, as the ones studied in this chapter, paramagnetic structures are fitted with singlets whereas ferromagnetic structures are fitted with sextets. In order to fit the spectra it is very important to know well the environment of the magnetic atoms. In a crystalline solid the iron atoms can be situated in different non-equivalent positions and therefore, their environments change. In this case, a different spectrum will be obtained from each non-equivalent iron atom and the resulting spectra will be the sum of the independent subspectra obtained for each non-equivalent iron atom. This may cause difficulties in separating the subspectra. When it is not possible to separate properly several subspectra, Mössbauer spectra can be fitted by a hyperfine field distribution, where non magnetic contribution is the central part around 0 T. The shape of the Mössbauer spectra supports the picture of a magnetic structure composed by ferromagnetic clusters surrounded by a paramagnetic phase. Figures 5.1 and 5.2 show the Mössbauer spectra obtained at several temperatures along with the corresponding hyperfine field distributions. The spectrum obtained at 77 K is composed mainly by a paramagnetic-like central contribution (peak around 0 mm/s velocity). Besides that contribution, the spectrum presents also certain not very formed ferromagnetic contribution joined to the central one. The ferromagnetic contribution evolves with temperature presenting soft out lines without marked transitions, and its contribution to the spectra shows up clearer and clearer as temperature increases. At the temperature of 200 K, two shoulders at both sides of the central paramagnetic peak around the 1mm/s and -1mm/s velocities are clearly appreciated. The shoulders become more evident as temperature increases and remain in all the spectra obtained at the higher temperatures. The distributions present two clear components.

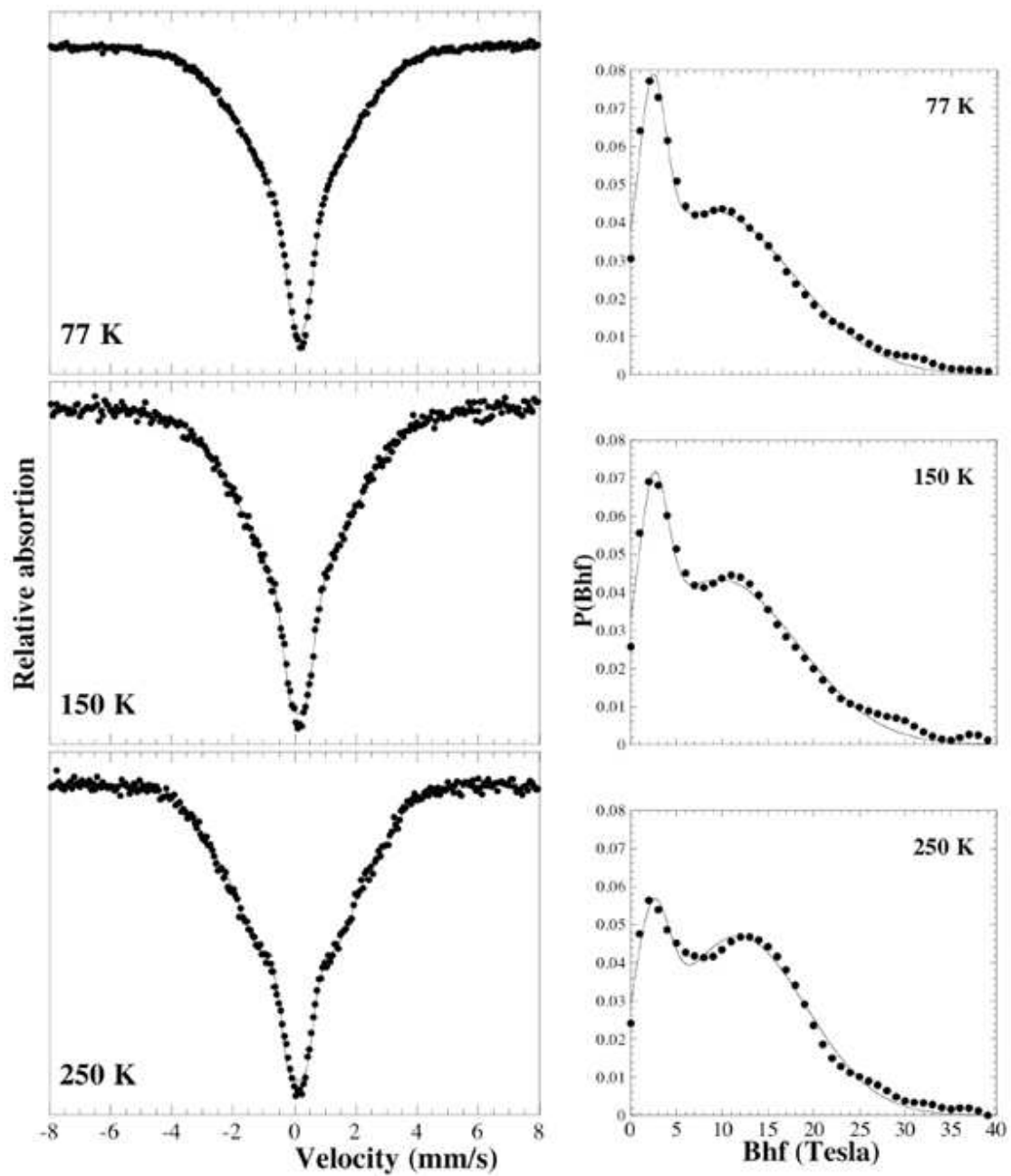


Fig. 5.1. Mössbauer spectra of the Fe<sub>70</sub>Al<sub>30</sub> alloy measured at 77 K, 150 K and 250 K. The curves on the right show the corresponding hyperfine field distributions.

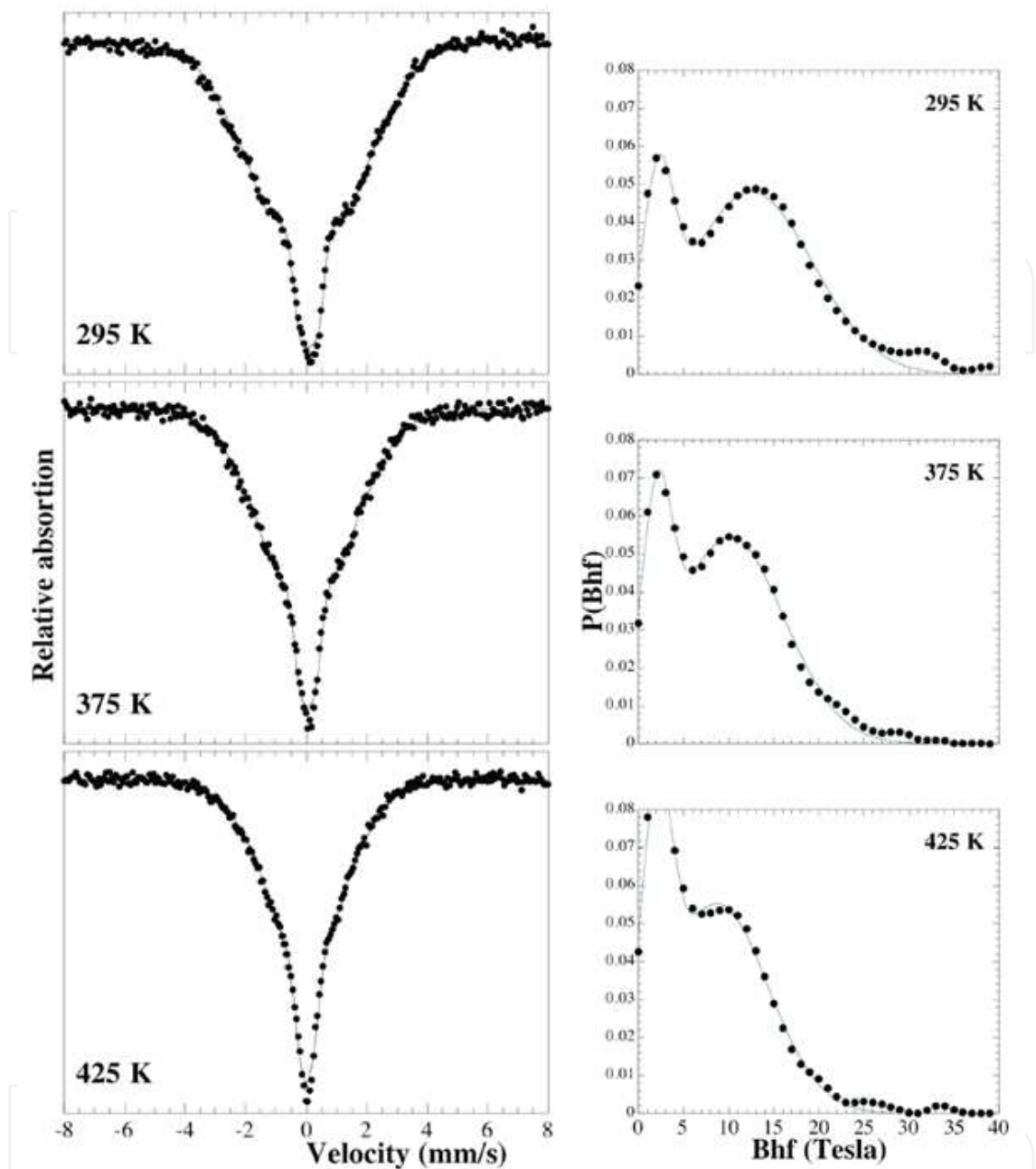


Fig. 5.2. Mössbauer spectra of the  $\text{Fe}_{70}\text{Al}_{30}$  alloy measured at 295 K, 375 K and 425 K. The curves on the right show the corresponding hyperfine field distributions.

One of them is located around two Tesla and it is associated with the paramagnetic-like contribution to the spectra. The second component is situated at higher fields and gives a description of the broad ferromagnetic contribution. Both components evolve with temperature. From figure 5.1, an increase of the high field component with temperature, at the expense of the low field component, is clearly observed and, at the same time, the maximum of the high field component shifts towards higher values. The scenario offered by figure 5.2 is just the opposite. In this temperature range, the component due to the ferromagnetic contribution decreases with temperature and the maximum returns to lower fields. A fitting of the hyperfine field distributions by means of two gaussians; one for each

component provides different and distinct information about the changes of both contributions to the Mössbauer spectra. Figure 6 shows the evolution of the intensity of the ferromagnetic contribution. The intensity of this component increases up to  $\sim 180$  K; from that temperature up, however, decreases monotonically. Figure 6 describes the relative changes with temperature of the quantity of ferromagnetic Fe atoms in the sample. Thus, the increase means that the number of ferromagnetic atoms increases with temperature up to  $\sim 180$  K, that is, up to the same temperature where the  $T_c^{inv}$  transition was observed in the ZFC-FC curves and within the temperature range where the maximum of the magnetic signal was observed in the  $M(H)$  curves of figure 3. From that temperature up, the intensity decreases. This can be interpreted as an evolution of the sample towards a more paramagnetic state. Mössbauer spectra confirm the results observed by Cable et al. [44]. Using a neutron diffuse scattering technique, they concluded that ferromagnetic clusters existed in the sample all over the regions observed in the ZFC-FC curve (figure 4) and the size of those ferromagnetic clusters was continuously increasing with temperature.

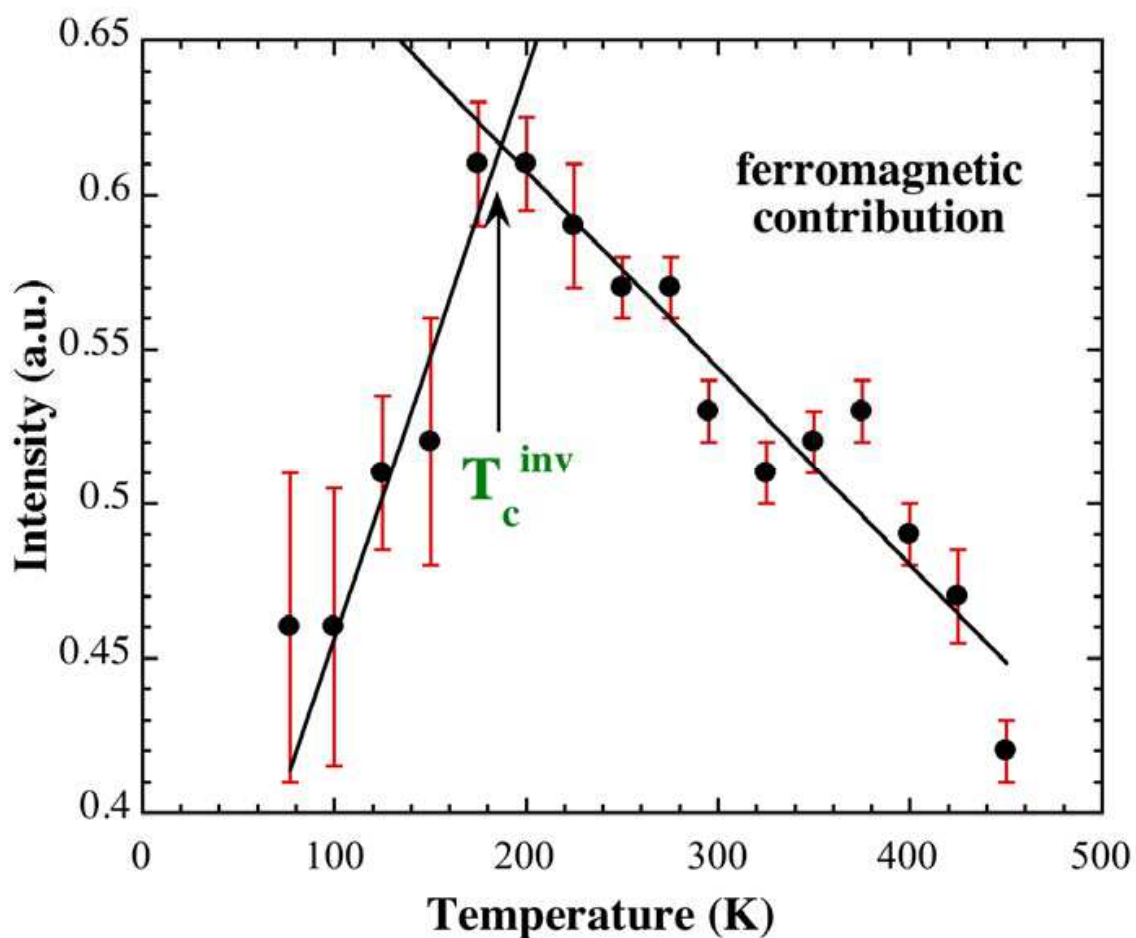


Fig. 6. Evolution with the temperature of the resonant area corresponding to the ferromagnetic contribution, as obtained from the fitting of the hyperfine field distributions of the Mössbauer spectra.

The most widely accepted model to explain the local magnetic character was firstly proposed by Srinivasan et al [45], and afterwards updated by Besnus et al. [8], and by Cable et al. [44]. Based on magnetic and neutron diffraction results, they proposed that the

magnetism is related to the local magnetic environment. They distinguished two kinds of Fe atoms, magnetic Fe atoms (those with four or more than four iron nearest neighbors) and paramagnetic Fe atoms (those with less than four Fe nearest neighbors), and their model basically consisted in the assignment of an adequate magnetic moment to each magnetic Fe atom. This model was very successful because it was able to explain qualitatively and quantitatively the effects such as the decrease of the magnetization signal with Al content in  $\text{Fe}_{100-x}\text{Al}_x$  alloys, the coexistence of the ferromagnetic and paramagnetic contributions in the Mössbauer spectra and the presence of ferromagnetic clusters in the sample. According to the model, the ferromagnetic clusters are the consequence of regions composed by Fe atoms with four or more than four Fe nearest neighbors, that is, regions formed by magnetic Fe atoms. In this sense, the evolution of the ZFC-FC curves of  $\text{Fe}_{70}\text{Al}_{30}$  alloy and the magnetic transitions observed in those curves (see figure 4) were explained as temperature dependent interactions between the paramagnetic phase and the ferromagnetic clusters due to the existence of random fields [46, 47].

The increase of the volume of the ferromagnetic phase and a probable increase of the quantity of magnetically interconnected clusters is behind the strong decrease of the slope value (see figure 7) observed between  $\sim 50$  K and  $\sim 180$  K, which is interpreted as a turning of the sample towards a more ferromagnetic state. The value of the slope changes again towards a constant value at  $T_c^{\text{inv}}$  temperature, which would mean that at that temperature, the sample has acquired its maximum ferromagnetic character.

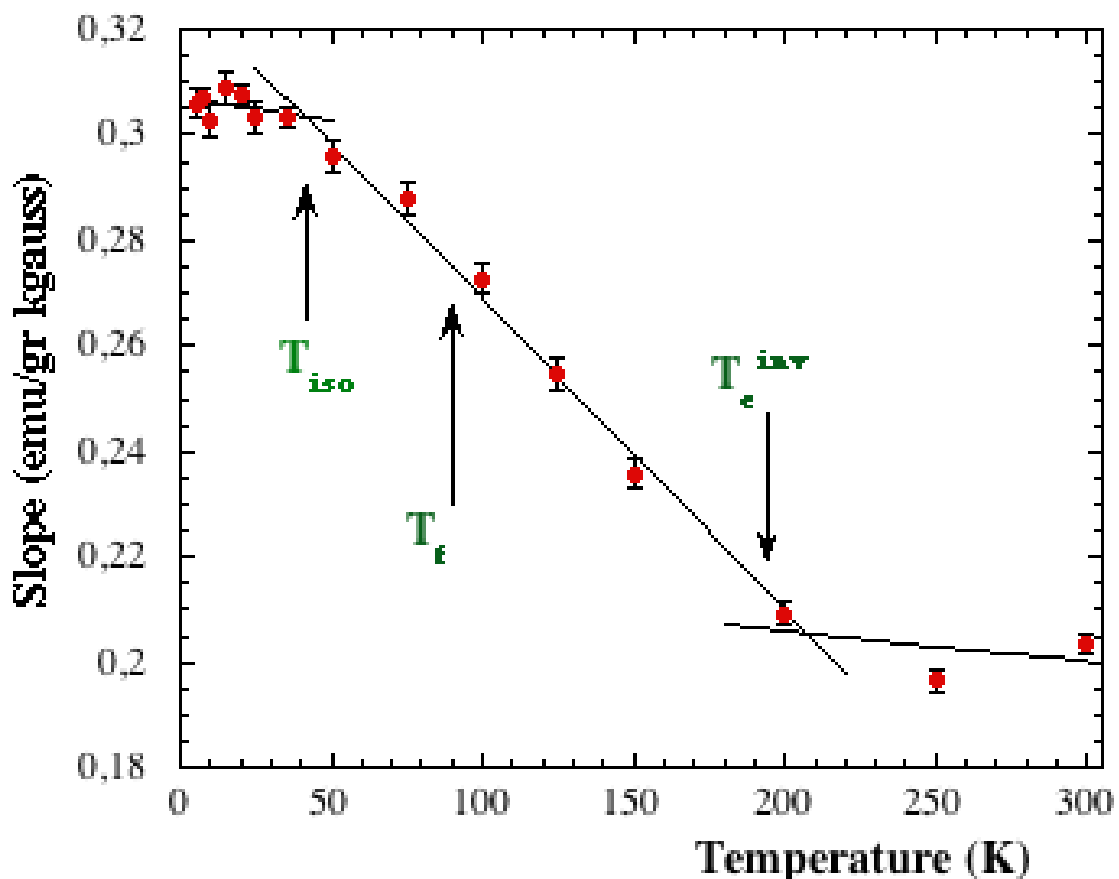


Fig. 7. Slope of the  $M(H)$  curves at high fields (between 4 and 7 T) versus temperature.  $T_c^{\text{inv}}$  and  $T_f$  are transition temperatures.

At  $T_c^{inv}$  the resonant area corresponding to the ferromagnetic component is 0.61, high enough for the clusters to be in physical contact, creating a ferromagnetic network in the sample by cluster interconnection. From that point on, posterior increase of cluster size might not imply an increase of the macroscopic ferromagnetic behavior of the sample and the value of the slope of the magnetization curves at high field remains constant.

Studies on magnetic fluctuations with temperature of the  $Fe_{70}Al_{30}$  ordered sample performed by neutron depolarization experiments show the same trend [41]. The average neutron polarization  $P_0$  decreased as the temperature increased and from  $T_c^{inv}$  temperature up it remained constant with a value close to zero. This change is explained as caused by the transition of the sample from spin-glass (cluster) state to the ferromagnetic state. Similarly, from inelastic neutron scattering data, published by Motoya et al. [38], it is observed that ferromagnetic spin-waves were formed above  $T_c^{inv}$  temperature. The authors interpreted that fact as an increase of the coupling degree between the spins of the paramagnetic region and the ferromagnetic network. Therefore, all these data suggest that  $T_c^{inv}$  transition is a consequence of the growth of the cluster size, but that the process related with the growth does not finish at that temperature.

The reentrant spin-glass state is defined as the entrance of the system to a spin-glass like state from ferromagnetism. In the  $Fe_{70}Al_{30}$  ordered sample, this state is formed below  $T_f \sim 90$  K temperature and it has usually been explained as the consequence of the total magnetic isolation of ferromagnetic clusters. The evolution of the ZFC curve with temperature (see Fig. 4) indicates that a magnetic disconnection of the clusters occurs, but also that such a disconnection is only effective while the applied field is zero.

### 3. Mechanically disordered alloys

#### 3.1 Volume expansion/Chemical disorder contributions

As mentioned above, the room temperature magnetic moment of ordered iron aluminides ( $Fe_{1-x}Al_x$ ) decreases slowly with increasing Al content, consistently with dilution models, up to  $x=0.2$ . With further dilution the magnetic moment decreases more rapidly, becoming zero for alloys with  $x \geq 0.35$  of Al [25]. However, disordered  $Fe_{1-x}Al_x$  alloys are ferromagnetic at room temperature even for alloys with  $x > 0.35$  [6, 14, 26, 48-56]. Thus, paramagnetic to ferromagnetic transition linked to an order-disorder transition can be observed after mechanical deformation. Experimentally, the influence of structural disorder on the magnetic properties has been evidenced in FeAl, in different types of microstructures such as cold worked single crystals [49, 26], quenched or cold worked polycrystalline materials [6, 8, 51], or ball-milled and mechanically alloyed systems [14, 26, 31, 48, 50, 52, 53, 55, 56]. From a theoretical point of view, the magnetism of diluted and disordered transition metal (TM) intermetallic alloys has been traditionally explained by the local environment model [10, 57]. In this model the magnetic moment of a given TM atom depends on the number of nearest-neighbor TM atoms: (i) either the TM atoms have their full moment when surrounded by a given minimum number of TM neighbors and zero otherwise [6, 8, 57] or (ii) the moment progressively decreases with reducing the number of TM nearest neighbors below a critical number [10, 48].

Using this simple model, the effect of Al substitution and disorder in FeAl can be qualitatively explained [6, 8, 10, 48, 57]. However, usually no quantitative agreement can be reached [6, 8, 10, 34, 48, 57-60].

It is noteworthy to take into account that the disordered state in FeAl alloys is accompanied by an increase of volume in the deformed state [14, 48, 50, 54-56]. Taking into account that variations in the distance between Fe atoms have profound effects on the magnetism [61-63], it was actually argued that the origin of the magnetic interactions in disordered FeAl intermetallics may not arise solely from nearest-neighbors magnetism (i.e., local environment model) but also from changes in the band structure of the material induced by lattice parameter variation ( $\Delta a_0$ ) [50, 14]. Actually, in the band structure calculations of disordered FeAl alloys an expansion of the lattice parameter is also found [27, 28, 64-67]. Moreover, there are clear indications from band structure calculations performed in  $\text{Fe}_{50}\text{Al}_{50}$  and  $\text{Fe}_{75}\text{Al}_{25}$ , that  $\Delta a_0$  could play a role in the magnetic moment of disordered FeAl intermetallics [68, 69]. Nonetheless, experimentally, the problem remained on how to separate disorder effects from  $\Delta a_0$  effects. One possibility was to reduce  $a_0$  by deformation without altering the disorder. For that purpose x-ray magnetic circular dichroism (XMCD) was studied in ball-milled  $\text{Fe}_{60}\text{Al}_{40}$  alloy under applied pressure, with the aim to separate the effects of disorder from those of lattice expansion on the magnetic properties [70]. The normalized XMCD integrated intensity (i.e. magnetic moment) and the normalized saturation magnetization do not practically change up to 1.4 GPa applied pressure (which corresponds to lattice parameter values of around 0.2905 nm; that is  $\Delta a_0/a_0 \sim 0.3\%$ ) (see Fig. 8). However, as the pressure is increased (the lattice parameter decreases) a magnetic phase transition is observed, leading to a rapid decrease of the normalized integrated XMCD

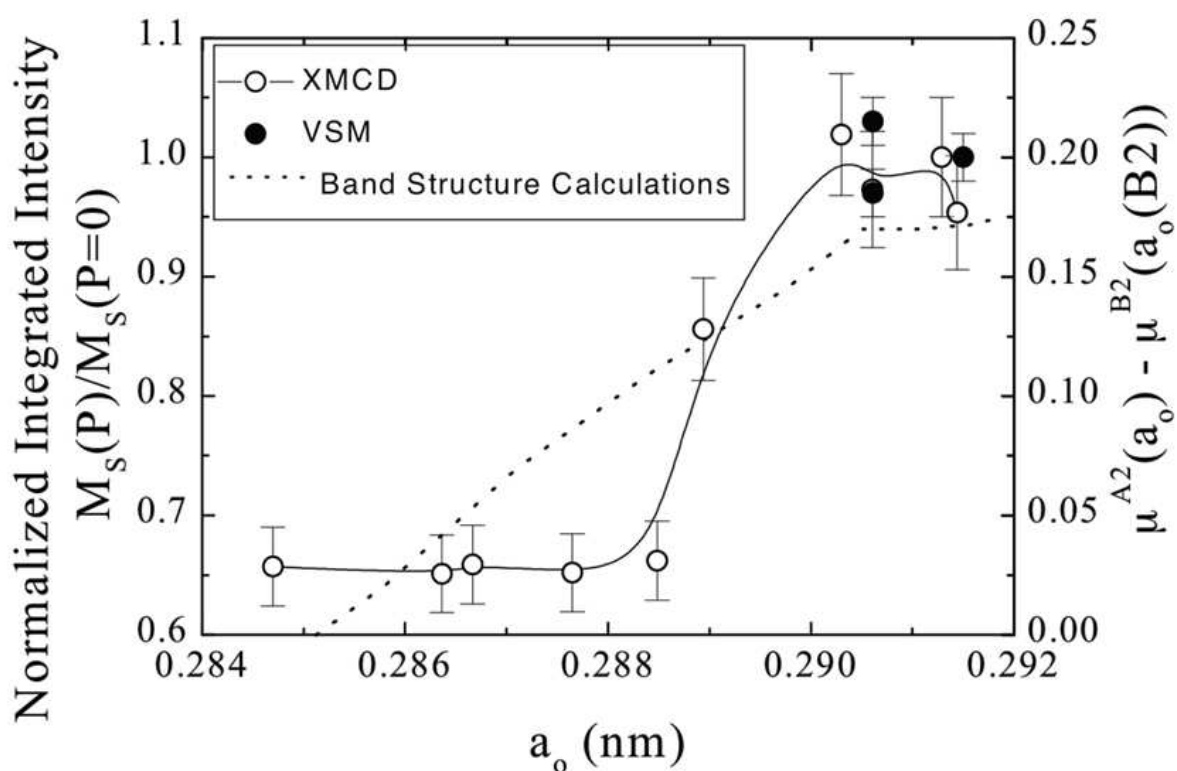


Fig. 8. Normalized XMCD integrated intensity (open symbols) and normalized saturation magnetization (filled symbols) vs the lattice parameter,  $a_0$ , for a ball milled  $\text{Fe}_{60}\text{Al}_{40}$  alloy. The dashed line shows the evolution of the theoretically calculated difference between the magnetic moment of the disordered alloy,  $\mu^{A2}$ , and the equilibrium magnetic moment of the ordered alloy,  $\mu^{B2}[a_0(B2)]$ , as a function of the lattice parameter,  $a_0$ , for a  $\text{Fe}_{62}\text{Al}_{38}$  alloy. The continuous lines are guides to the eye. Figure taken from reference [70].

intensity (i.e. magnetic moment) reaching a value that does not change with further pressure. This indicates that when the lattice parameter  $a_0$  reaches approximately the one of the ordered sample, then up to  $35\pm 5\%$  of the magnetic moment of the sample vanishes. This sharp magnetic transition indicates the existence of a moment-volume instability, which is not related to any structural phase transition, because XRD measurements do not show any phase transition in the studied pressure range. The band structure calculation results shown in figure 8 give a contribution of volume change ( $\Delta a_0$ ) to the total magnetic moment of about  $45\pm 10\%$ ; which is intermediate between the ones calculated in  $\text{Fe}_{50}\text{Al}_{50}$  and  $\text{Fe}_{75}\text{Al}_{25}$  [68]. Therefore, experimental and theoretical results demonstrate that the magnetism in this kind of system arises from both the atomic disorder and the disorder-induced lattice expansion. This is in contrast to previous studies where only near-neighbor effects were considered to explain the magnetic behavior of similar alloys. In the case of disordered  $\text{Fe}_{60}\text{Al}_{40}$ , experimentally, the contribution of disorder and lattice expansion account for 65% and 35% of the magnetism of the alloy, respectively.

### 3.2 Disorder process

Once having studied the volume effect on the magnetic properties of disordered alloys let's tackle the study of the disordering process as a whole. The  $\text{Fe}_{70}\text{Al}_{30}$  alloy was chosen to systematically study and characterize the evolution of different surroundings of Fe atoms with mechanical deformation (milling time), during the order-disorder transition. This alloy presents a weak magnetism at room temperature (see section 2) [71].

XRD measurements performed at room temperature on the  $\text{Fe}_{70}\text{Al}_{30}$  alloy show that with ball milling a complete transition from the ordered alloy to the disordered one is obtained. The area of the (100) superstructure peak decreases with milling time, up to 5 h (see Fig. 9), when it disappears, and then only the disordered A2 phase can be distinguished. Fig. 9 shows a progressive lattice parameter increase that reaches a maximum after six milling hours. The maximum lattice parameter increase in the order-disorder transition amounts to 0.7%, which is in good agreement with the volume increase obtained after deformation in alloys in the range 27.5-35 at% Al [32].

DTA measurements show an exothermic peak at about 200 °C for samples milled for more than 1 h (see inset of Fig. 10). Figure 10 shows the evolution of the enthalpy, obtained from the integration of the exothermic peak, with milling time. The enthalpy increases up to 6 h of milling when it saturates. Taking into account the previous XRD measurements that show a complete transition from the ordered phase to the A2 disordered one for milling times larger than 5 h, the calorimetric peak is attributed to structural reordering of the sample. That is to say, the larger the area of the exothermic peak the larger the disorder of the ball milled sample. At 6 milling hours the enthalpy saturates; therefore, it can be concluded that after 6 milling hours a complete disorder is obtained (see Fig. 10). It is worth mentioning that in the 1-hour milled sample no peak can be distinguished at 200 °C.

Therefore, the calorimetric data, consistent with XRD data, indicate that the disordering process in the transition between the ordered alloys to the completely disordered one is a progressive one. With milling time the A2 phase starts forming (growing enthalpies) and it goes on increasing till the entire sample gets the disordered A2 structure.

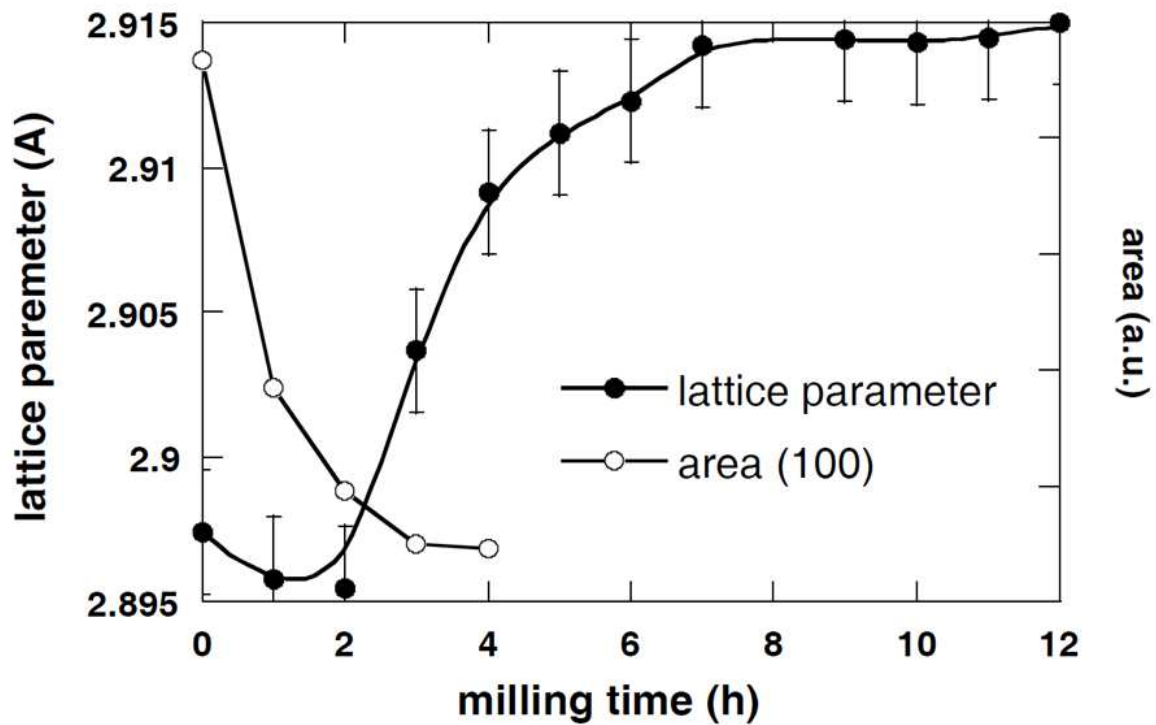


Fig. 9. (100) superstructure peak (empty circles) and lattice parameter (full circles) evolution with milling time. The solid lines are guides for the eye. Figure taken from reference [71].

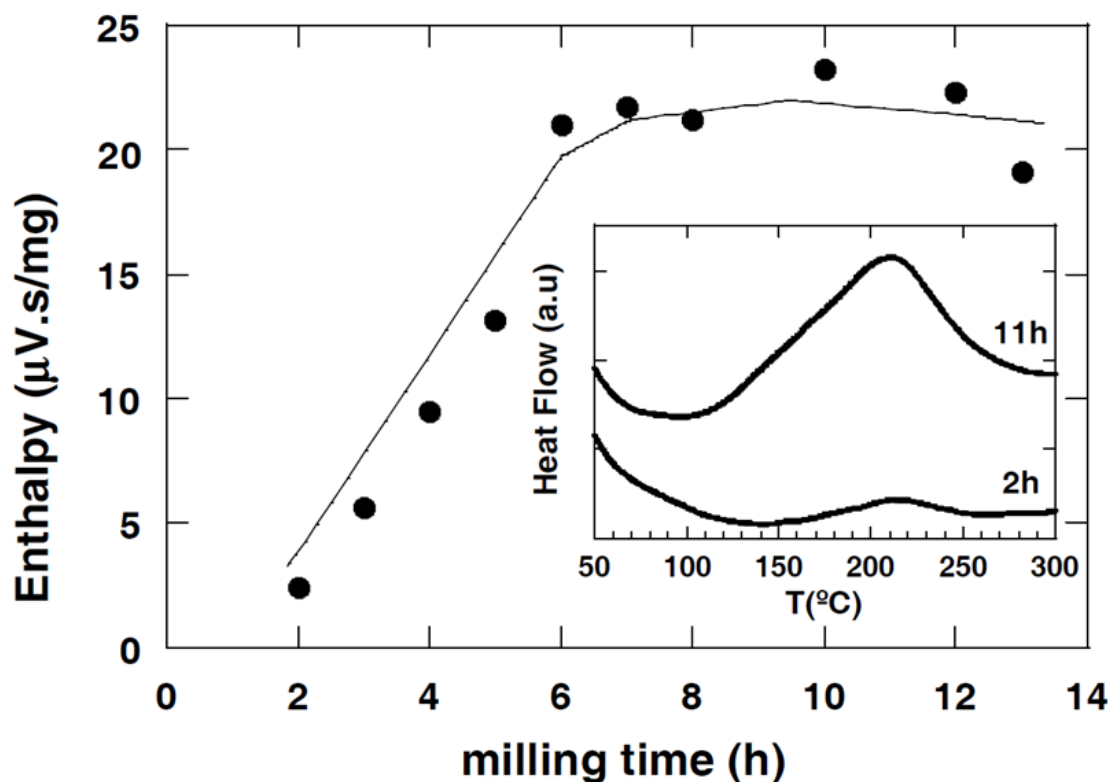


Fig. 10. Evolution with milling time of the enthalpy of the exothermic peak obtained around 200 C in the DTA (the solid line is a guide for the eye). The inset shows the calorimetric data obtained for samples milled for 2 and 11 h. Figure taken from reference [71].

Fig. 11 shows magnetization curves for different milling times [72]. The figure shows an abrupt magnetic property change from four to five milling hours, which is also observed in Fig. 12 [72]. The magnetization value obtained at applied fields of 7 T measured at 10 K (see Fig. 12) indicates clearly that before complete disorder is obtained in the samples (X-rays indicate that this happens after five milling hours) magnetic saturation is not reached at 7 T. Once complete disorder is obtained, (above 5 h of milling time) magnetic saturation is reached at around 4 T. In addition, Fig. 12 shows clearly the increase of magnetization with disorder. The shape of the magnetization curves for few milling hours (less than 5 h) is similar to the one of the annealed sample; this indicates that there is still order in those samples. It is interesting to indicate that even though the XRD and calorimetric data indicate a monotonous increase of the disorder with the milling time, the magnetic data (see Figs. 11 and 12) show an abrupt change between 4 and 5 h of the milling time.

Figure 13 shows the Mössbauer spectra measured at room temperature for samples milled for different times. The annealed sample presents a large paramagnetic contribution superposed on a wide non-defined magnetic one. After the first milling hour, the paramagnetic contribution decreases and broadens and the wide magnetic contribution is yet to be defined. After 3 h of milling (even after 2 h) the magnetic contribution starts to be defined and a wide sextet-like contribution starts to appear superposed on a paramagnetic contribution. Therefore, in order to fit the spectra of Fig. 13 left a hyperfine field distribution,  $P(B_{hf})$ , was used. However, it is not until the samples are milled for 4 or more hours that the spectra show a clear sextet (see Fig. 13 right). Therefore, the fitting of the spectra of Fig. 13 right (4 or more milling hours) has been performed with a singlet and discrete sextets. Fig. 14 shows, in the case of samples milled for less than 4 h the  $P(B_{hf})$  obtained fitting the spectra. In the case of samples milled for 4 h or more, besides the discrete sextet fittings, in order to compare them with the ones performed for alloys milled during shorter time, we have made also fittings with hyperfine distributions in the spectra up to 5 milling hours (see figure 14).

In the annealed sample the  $P(B_{hf})$  shows two main peaks at low fields (around 2 and 10 T) and a very small one at 28 T. Evidently, the peak located at 2 T must correspond to the paramagnetic contribution of the spectrum. After the first milling hour the pattern is similar but the  $P(B_{hf})$  shows a clear evolution, although the first two peaks are still present, the peak at 2 T decreases quite significantly and a wide bump around 28 T appears (it is worth mentioning that in the calorimetric measurements no meaningful difference between the annealed and 1 h milled sample was obtained). The evolution continues monotonically with the milling time and already after 3 h of milling the main contribution to the spectrum comes from the bump centered at 28 T. The  $P(B_{hf})$  of the spectra milled up to 3 h can be fitted using three Gaussians. However, three Gaussians are not enough to fit the  $P(B_{hf})$  of the spectra with more milling hours, which is another indication of the magnetic order increase with milling time; and indicates that the proper fitting of those spectra must be made discretely.

As the value of each sextet depends on the environment of each iron atom, the discrete fitting of the spectra with 4, 5, 6 and 11 milling h (see Fig. 14) has been performed using six sextets and one singlet. Each sextet corresponds to Fe atoms that have a fixed number of Fe nearest neighbors in a bcc structure, like the disordered A2 one. Figure 14 shows that the peaks of the  $P(B_{hf})$  built out of the discrete fit (each peak corresponds to a Gaussian that has

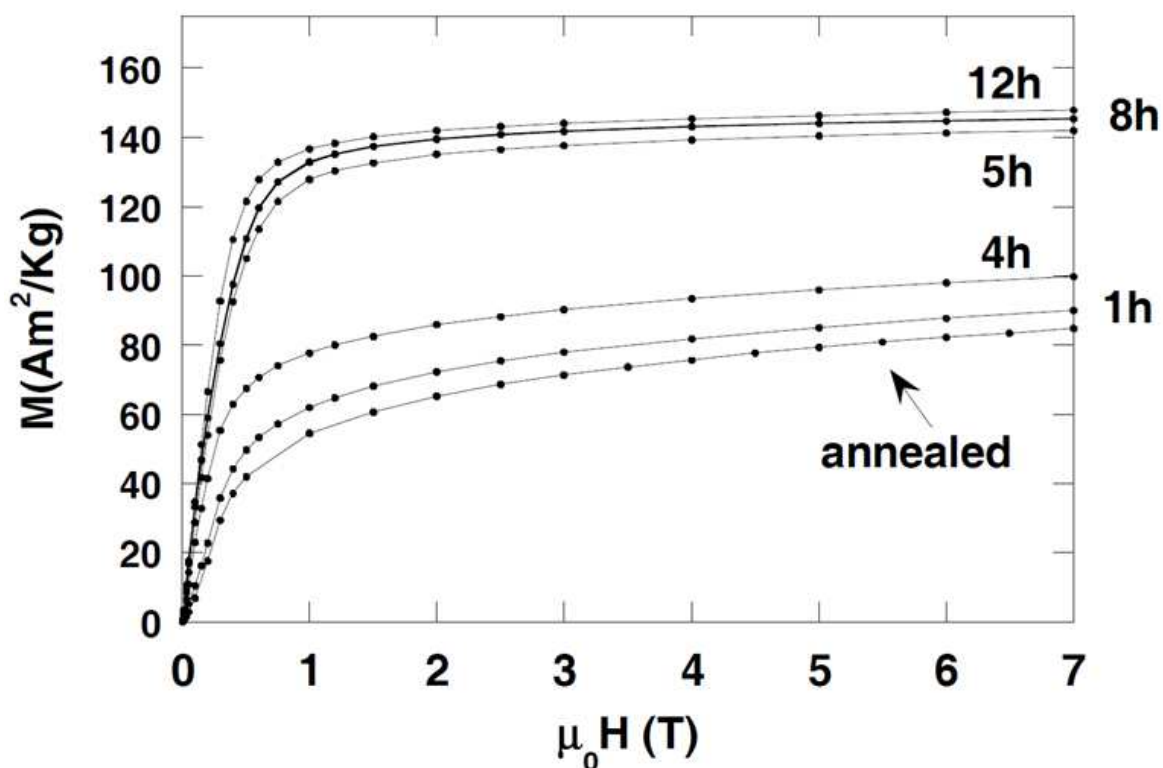


Fig. 11. Magnetization curves at 10 K for samples milled for different hours. Figure taken from reference [72].

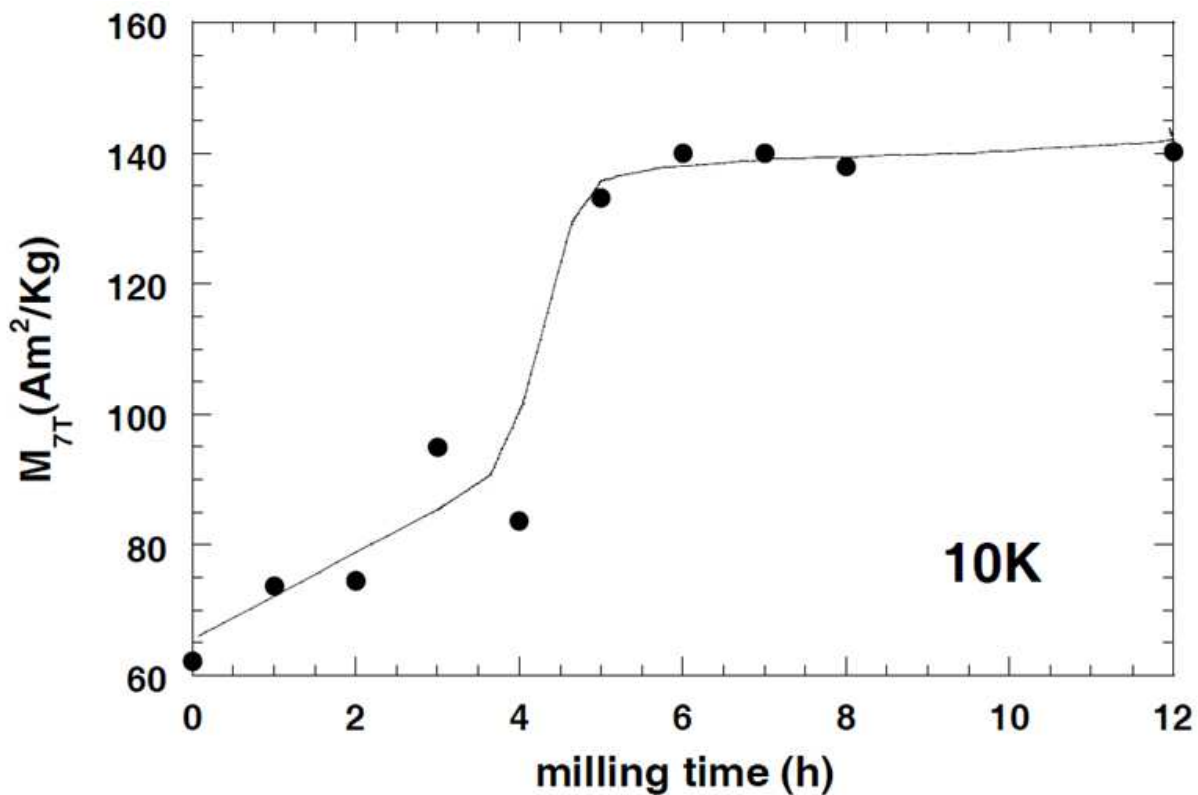


Fig. 12. Magnetization of  $\text{Fe}_{70}\text{Al}_{30}$  alloy measured at 10 K and 7 T versus milling time.

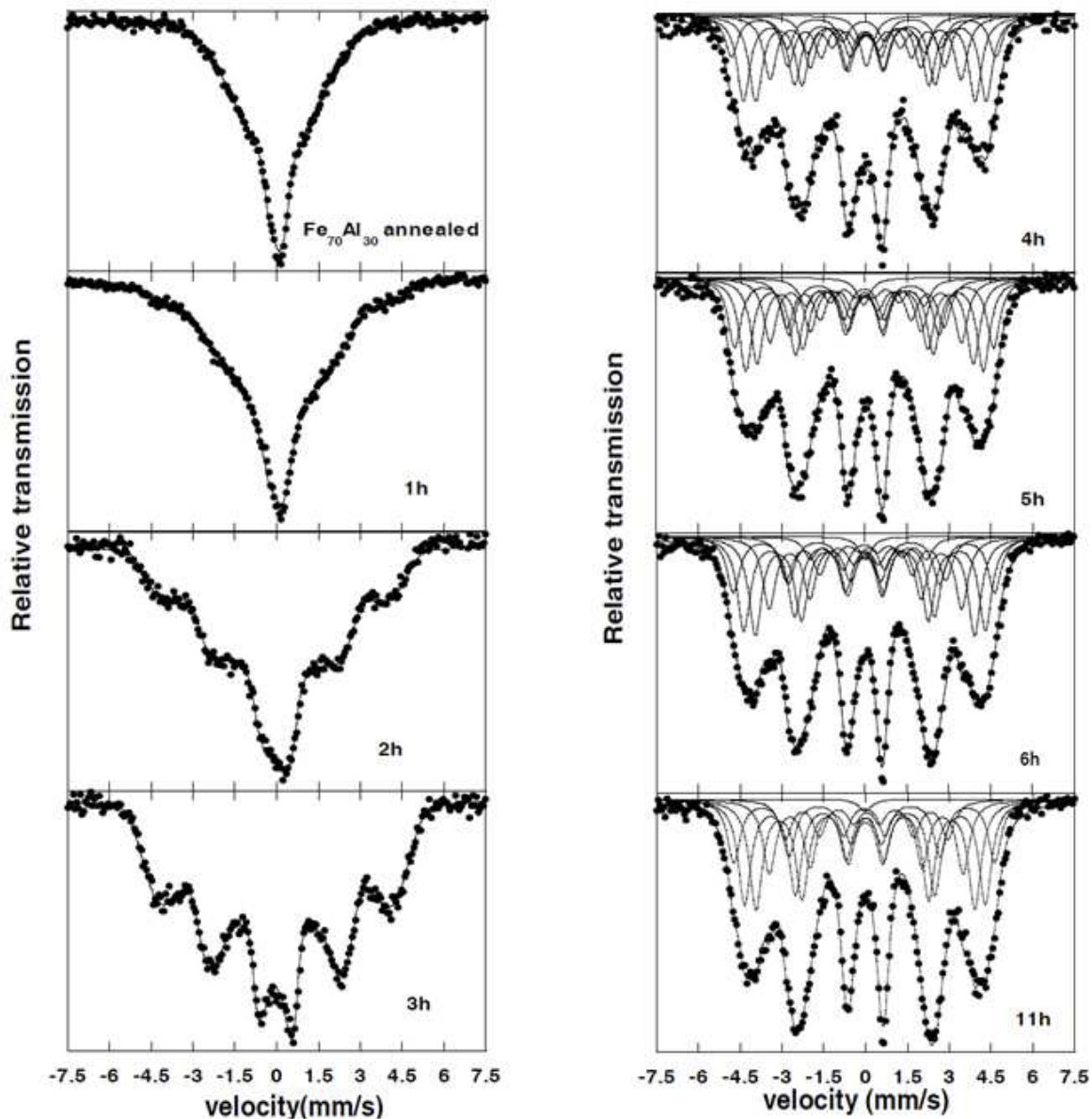


Fig. 13. Mössbauer spectra measured at RT in  $\text{Fe}_{70}\text{Al}_{30}$  alloy after different milling time.

been built taking into account the width and area of each subspectra obtained from the discrete fits) correspond very well to the values inside the second and third bumps of the  $P(\text{Bhf})$  distribution. Besides, Fig. 14 shows that the area of the peaks (corresponding to sextets), with  $\text{Bhf}$  lower (larger) than 20 T, decreases (increases) with milling time. Indeed, at long milling hours the peak around 10 T disappears. Therefore, the main magnetic contribution to the spectra in the annealed and short time milled samples disappears completely in the completely disordered state. On the other hand, the small magnetic contribution centered around 28 T, present in the annealed sample, seems to be the seed of the main contributions obtained in the completely disordered samples. Moreover, the area of the sextet used in the fitting of a completely disordered alloy (11 h of milling time) agrees quite well with the shape of the binomial distribution corresponding to the A2 structure of  $\text{Fe}_{70}\text{Al}_{30}$ [72].

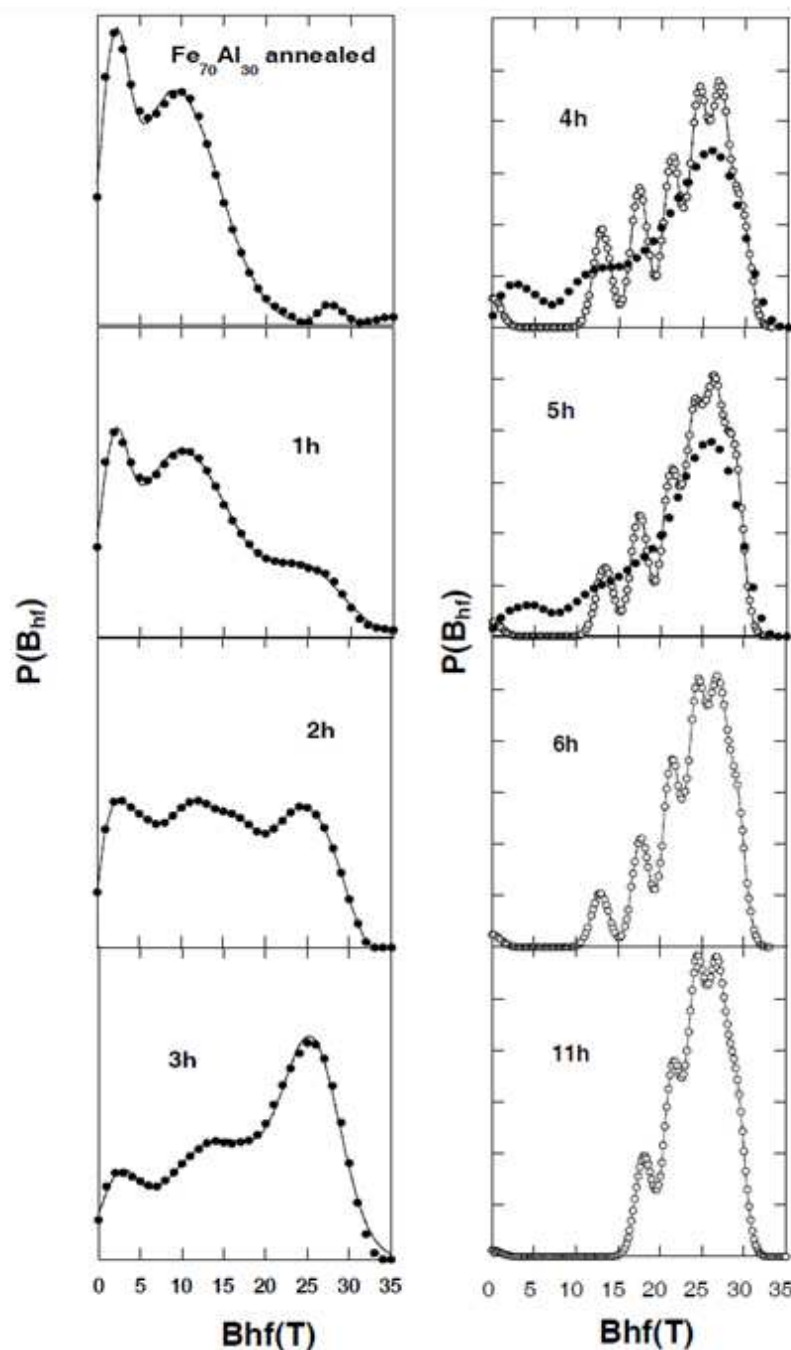


Fig. 14. (Full circles)  $P(B_{hf})$  of the hyperfine field distribution obtained from the fit of Mössbauer spectra of Figure 11. (Empty circles) simulated  $P(B_{hf})$  from the discrete sextets fit of the spectra (see text).

Summarizing, the different techniques show that the milling is a dynamical process. The ball milling causes the structural order-disorder transition in the sample and a lattice parameter increase that amounts to 0.7%. At the same time magnetic order is induced in the alloy.

The experiments performed indicate that the order-disorder transition is a monotonous process from the structural point of view that (in our conditions) this transition is accomplished completely after 6 milling hours. However, the magnetization shows an

abrupt change at low temperature before complete disorder takes place. The Mössbauer spectra suggest that the main contribution of the weak magnetism of the ordered sample disappears and that the small contribution is the seed of the enhancement of the magnetism in the order-disorder transition. Moreover, the area of the sextet used in the fitting of the completely disordered alloy agrees with the shape of the binomial distribution corresponding to the A2 structure of Fe<sub>70</sub>Al<sub>30</sub>.

#### 4. Reordering of disordered alloys

In the former subsection the effect of mechanical deformation on the magnetic properties of Fe-Al alloys has been shown. The overall effect of the deformation on the sample was the induction of a disordered state that follows the binomial distribution, corresponding to the A2 disordered structure, and volume expansion. The amount and type of deformation can determine the change on the magnetic signal of the sample, even causing a transition between paramagnetic and ferromagnetic behaviors (or from paramagnetic to ferromagnetic state). However, this transition is metastable and the former state can be recovered just by heating the sample. The processes involved are called *recovery and recrystallization processes* [73]. As the deformed state has locally many defects and each kind of defect has its own thermal activation temperature, this process is not monotonous and it usually occurs in several stages. When appropriate temperature is reached for some type of defect, the mobility of the defects is activated and they migrate to the surface where they disappear. It is evident that the smallest defects, like point defects, need smaller energy to migrate; therefore, these are the type of defects that are going to be removed first when the sample is heated. Larger defects, like planar defects (antiphase boundaries (APB)), will need higher energy to be moved, and their activation temperature will be higher. The study of these processes and its influence on the magnetic properties of the studied alloys can be important to identify which defects are important in the change on the magnetic properties, and more particularly, in the case of Fe-Al alloys.

The studies found in literature show that in the case of the Fe-Al binary alloy system two stages have been found for alloys in the B2 phase field independent of the type of deformation applied to the samples: cold rolled [26, 74], ball milled [14, 50, 54] or crushed (ours). The first stage takes place around 400-500 K. During this stage a peak has been observed in calorimetric measurements [26, 54, 71], and neutron diffraction patterns [75] show a nucleation of new small ordered domains with B2 structure accompanied by a decrease of the lattice parameter. The second stage takes place between 600-700 K when the defects introduced during deformation disappear completely. In this stage, the B2 domains present in the alloys start to grow until all the strains in the sample are released by annealing [75].

In the case of alloys in the D03 field of the phase diagram, the recovery process occurs through the creation of transient B2 phase. In fact, the two stages are the same as in the case of D03 [76]: nucleation of small B2 domains in the first stage and growth of the existing B2 domains in the second one. However, in this case growth of the existing D03 domains takes place immediately after the second stage a domain.

In both cases (B2 and D03), the recovery processes follow the phase transformations described in the classical work by Allen and Cahn [77].

The influence of these processes is very strong due to the recovery of the intermetallic order. Fig. 15 shows the magnetization as a function of temperature for different mechanically deformed Fe-Al alloys with an applied field of 0.15 T. In the case of alloys in the B2 field of the phase diagram (35 at. % Al), the magnetization drops to zero in a single stage, and this occurs around 400-500K. This large drop of magnetization takes place simultaneously with the first stage of the recovery process, described above [54, 75, 76]. After this, the contribution of the remaining deformations in the alloy is negligible.

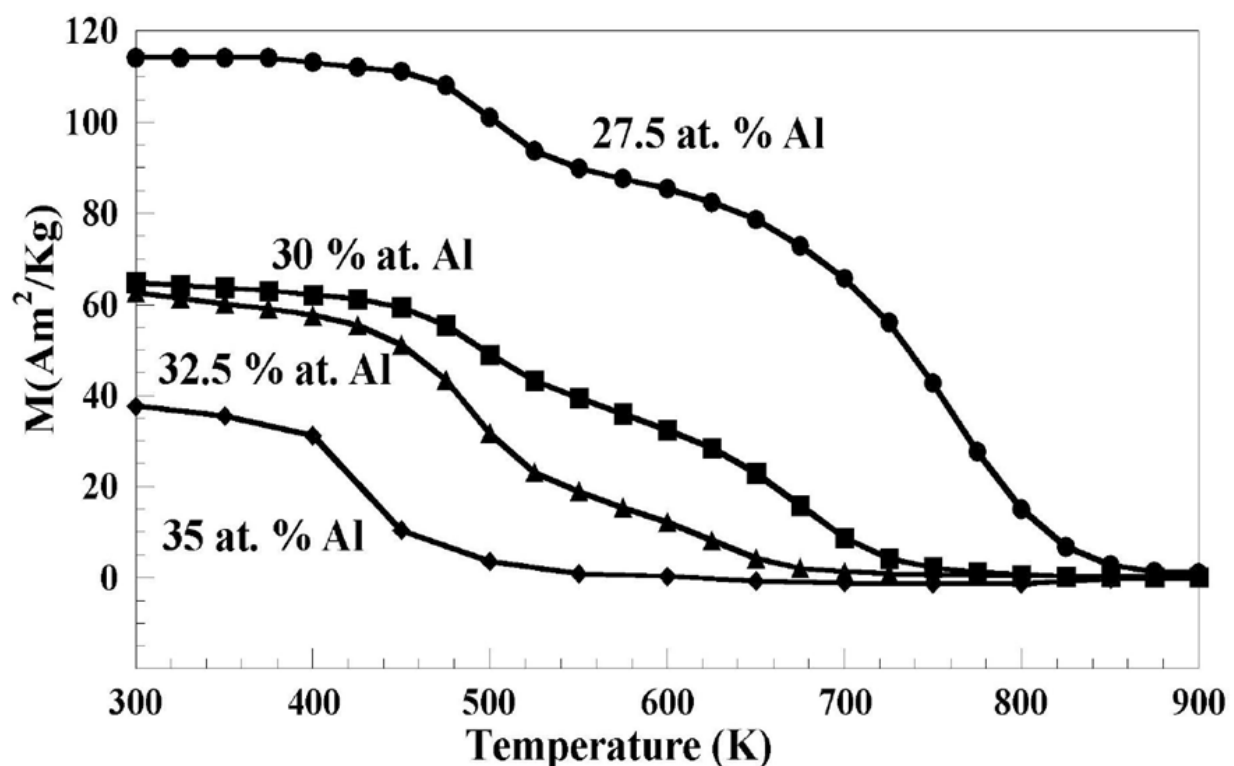


Fig. 15. Magnetization as a function of temperature of mechanically deformed alloys with an applied field of 0.15 T. The deformation of the alloys is explained in refs. [75] and [76].

Mössbauer spectroscopy measurements also show the same image, as can be found in figure 16. This figure confirms that after the first stage there is no magnetic contribution [75, 76]. In the case of alloys with D03 structure the magnetic evolution is different. There is a marked drop in magnetization around 400-500 K, however this time the magnetization does not drop to zero. Mössbauer spectroscopy measurements also show magnetic contributions after this stage in the recovery process. The magnetization in alloys with D03 structure will drop to zero around 800 K.

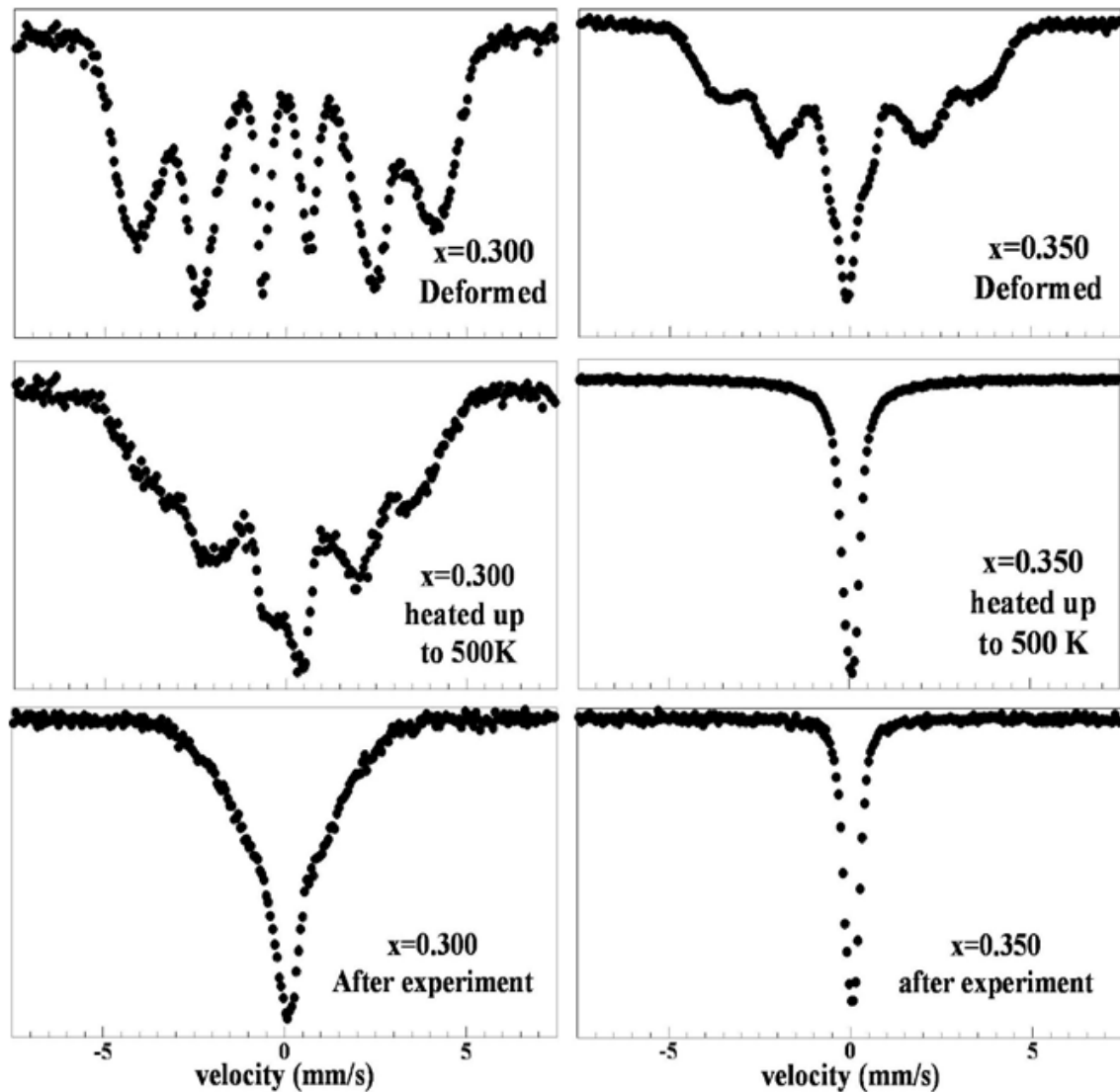


Fig. 16. Mössbauer spectra of alloys with 30 (left) and 35 (right) at. % Al in different situations: (top) mechanically deformed, (middle) heated up to 500 K (i. e., after the first stage in the recovery process), (bottom) heated up to 900 K (i. e., after the second stage in the recovery process). From references [75] and [76].

According to the process described above, the first stage in the recovery process of alloys with B2 and/or D03 can be attributed to removal of some kind of defect that causes an increase in volume of the lattice. Furthermore, this kind of defect also causes a strong increase in the magnetic signal. In literature this stage has been attributed to the removal of point defects [54, 76] like vacancies, and this is plausible, as the energy necessary to move this kind of defects is low. On the other hand, studies performed on cold rolled alloys [10, 74, 77] attribute this stage to APB tube [79, 80] removal. However, these two explanations are compatible since the APB tube removal takes place by means of vacancy migration [26]. The second stage in the recovery process, on the other hand, must be due to removal of larger defects. In literature, this has been attributed to removal of planar defects [54] and more specifically to superdislocations [26]. It is also important to remark that according to the work on cyclically deformed alloys performed by Yasuda et al. [81], the main

contribution to the magnetic signal comes from APB tubes and superdislocations' contribution is negligible. In the case of alloys with D03 structure, there is still a strong magnetic signal remaining in the alloys after the first stage. As stated above, the superdislocations on B2 domains have no significant magnetic contribution, and therefore this remaining magnetic signal must come from the existing D03 domains. However, these D03 domains must be deformed because the Curie temperature of the alloy with 30 at.% Al is around 500 K and at that temperature the signal is still strong.

All the processes described allow us to study the effect of the Fe local environment and the Fe-Fe interatomic distance on the magnetic properties of Fe-Al alloys. Up to now, this influence for Fe-Al alloy system was focused on the magnetic moment, but taking into account the spin-glass properties, found in this alloy system (see section 2), there must exist an influence on the competition between ferromagnetic and antiferromagnetic exchange interactions. This influence on the exchange interactions has been used to explain the Invar effect on Fe-Ni alloys [82] and has been proven in Fe-R (R=rare earth) alloy systems [83].

This can explain the fact that for B2 alloys, the strong drop of magnetization in the first stage of recovery takes place due to the decrease in volume, because after this stage, the intermetallic order is not completely recovered and its magnetic contribution is negligible. This indicates that in the case of alloys in the B2 phase field of the phase diagram, the change in volume contributes in a higher degree than the change in Fe local environment. However, in the D03 alloys, the magnetic contributions do not disappear after the first stage. The only difference in this case is the presence of domains with D03 structure. In this case, as the D03 structure has more Fe-rich local environments, the changes in Fe local environment due to the deformation will lead to Fe-richer Fe-local environments. Therefore, both changes in Fe-Fe interatomic distance and in Fe local environment have an important influence.

In summary, the studies of the recovery process in deformed Fe-Al alloys demonstrate that both the Fe local environment and the Fe-Fe interatomic distance can be responsible for the origin of magnetism in Fe-Al alloys.

## 5. Theoretical calculations

Because of the great difficulties in understanding these compounds and the interesting properties they show, during the last years the band calculation has been used to study this system.

The electronic structure of magnetic transition-metal (TM) aluminides with stoichiometric composition has already been studied many times by various methods and in different approximations. In the earliest calculations within the Korringa-Kohn-Rostoker (KKR) [84] and modified KKR methods [85-87] the problem of filling up of the transition metal (TM) d-bands by Al p-electrons was discussed in detail and the charge transfer from Al to a TM site was shown. The trends in the chemical bonding and the phase stability of transition metal aluminides with equiatomic composition have been studied with the full-potential linearised augmented plane-wave (FLAPW) method [88]. A review of electronic structure calculation results, along with band structures, densities of states and Fermi surfaces of many TM aluminides can be found in ref. [89]. Another study using the full-potential linearized augmented Slater-type orbital method [90] reports the formation energies and equilibrium volume of many 3d aluminides. In addition, cohesive, electronic and magnetic

properties of the transition metal aluminides have been calculated using the Tight Binding Linear Muffin Tin Orbital (TB-LMTO) method [91] where it was found that FeAl retains its magnetic moment. These findings coincide with the results of earlier Linear Muffin Tin Orbital (LMTO) calculations for NiAl and FeAl intermetallic compounds [92]. In all these calculations for the Fe<sub>50</sub>Al<sub>50</sub> stoichiometric composition a magnetic moment was found, but Mohn et al. [93] found a non-magnetic ground state for this alloy and composition using corrected Local Density Approximation (LDA+U).

On the other hand, there are relatively few calculations aimed at the study of the influence of defects on the electronic and magnetic structure of TM aluminides. The LMTO method has been applied to study the electronic structure of antisite (AS) defects in FeAl where point defects were modeled by suitably chosen supercells [94]. Finally, the Linear Muffin Tin Orbital Coherent Potential Approximation (LMTO-CPA) technique has been used to discuss the order-disorder transition in FeAl alloys [29]. The supercell approach has been used in order to study the antiphase boundary in NiAl and FeAl [95], as well as point defects in these aluminides [96]. The onset of magnetism in Fe-Al system as a function of the defect structure was studied using the CPA within the KKR method for the disordered case and the TB-LMTO for the intermetallic compound [27], where they found appearance of large local magnetic moments associated with the Fe antisite defect.

In our work we mainly performed calculations based on TB-LMTO in order to study these alloys, and the results we obtained are useful in giving an idea of the general trend of the magnetism in these alloys. Nowadays, the Vienna Ab-Initio Simulation Package (VASP) with a wide choice of potentials is commonly used and this is why we decided to perform some tests with this method in order to see what results could be obtained. This latter method is more time consuming, which is a disadvantage when making supercell calculations; however, it allows introducing vacancies as well as ion relaxation in a simple way and it could be useful for the study of these alloys.

In the previous sections we have studied experimentally the cause of the large change in the magnetic properties with structural transition and the increase of the magnetic signal with the temperature observed in ordered Fe<sub>70</sub>Al<sub>30</sub> sample. Theoretical calculations are very useful in order to understand the mechanism that leads to these changes of magnetic properties.

We study ordered (A2, B2, D03, B32) and disordered (B2) structures present in the Fe-Al phase diagram for different Fe compositions. Moreover, the influence of disorder on the magnetic properties of the Fe-Al system is also studied. Details on these calculations are given in ref. [28].

We calculated the lattice parameter, the total energy, the cohesive energy, the density of states (DOS), the magnetic moment and other interesting data that will be shown in this work. We performed the calculations both for non-polarized and spin-polarized cases. First, we got the convergence for non-polarized calculations and then we divided the moments and potentials into two, one belonging to each spin, and we made the calculations again for these new values. It is worth mentioning that, as shown in figure 17, in most of the structures studied the spin-polarized cases showed a lower energy, and therefore it can be said that this system is magnetic for most of the studied cases.

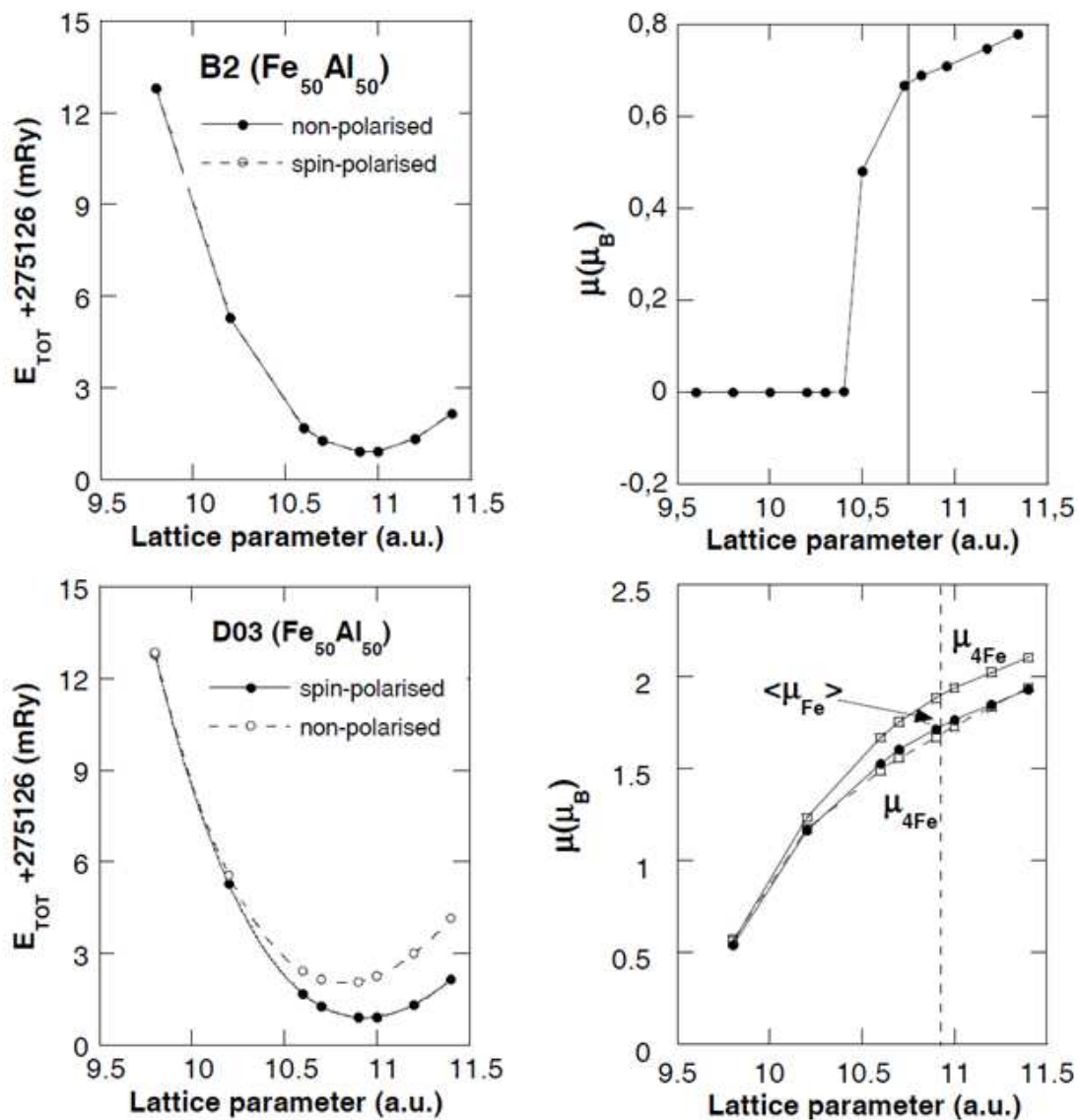


Fig. 17. (a) Energy and (b) magnetic moment evolution with lattice parameter. The experimental lattice parameter for Fe<sub>50</sub>Al<sub>50</sub> alloy is almost 1% larger than the one calculated theoretically in this work, in agreement with the general experience that local density approximation (LDA) underestimates the lattice parameter (see Table II). Figure taken from reference [28].

### 5.1. Ordered structures

Three different ordered structures have been studied B2, D03 and B32 for different compositions. We first analyzed the Fe<sub>50</sub>Al<sub>50</sub> thoroughly and used these conclusions to explain the results of the other compositions. Also, the study helps in understanding the influence of the nearest neighborhood of Fe sites on its magnetic properties in different structures.

Table I shows the results obtained and table II presents a comparison between the experimental values of Fe<sub>75</sub>Al<sub>25</sub> and Fe<sub>50</sub>Al<sub>50</sub> compositions with the theoretical ones obtained by different authors for the structures and compositions shown in the phase diagram.

The calculations performed for the B2 structure and Fe<sub>50</sub>Al<sub>50</sub> composition are in very good agreement with the results that appear in the literature [27, 90, 91, 97].

Composition	Structure	a (a.u.)	B (Gpa)	$\mu_{Fe}(\mu_B)$	$E_{coh}(eV)$	$E_f (eV)$	$E_{min}(eV)$
Fe <sub>50</sub> Al <sub>50</sub>	B2	10.74 (10.77)	200	0.64	-5.91	0.462	-3743.302 (-3743.301)
	D03	10.93 (10.82)	173	1.71	-5.66	-0.204	-3743.258 (-3743.240)
	B32	10.91 (10.82)	44	1.67	-5.73	-0.286	-3743.270 (-3743.244)
Fe <sub>75</sub> Al <sub>25</sub>	B2	10.6 (10.50)	192	1.07	-6.25	-0.245	-4086.982 (-4086.966)
	D03	10.65 (10.51)	176	1.86	-7.62	-0.252	-4086.984 (-4086.969)
	B32	10.71	190	1.97	-6.18	-0.171	-4086.913
Fe <sub>81.25</sub> Al <sub>18.75</sub>	D03	10.63 (10.47)	197	1.90	-6.31	-0.177	-4153.892 (-4153.871)
Fe <sub>87.5</sub> Al <sub>12.5</sub>	B32	10.62 (10.43)	208	2.02	-6.38	-0.180	-4215.130 (-4215.101)

Table I. Summary of the results obtained for the ordered structure, where  $a$  is the lattice parameter,  $B$  the bulk modulus,  $\mu_{Fe}$  the mean magnetic moment per Fe atom,  $E_{cohe}$  the cohesive energy for the spin-polarized calculations,  $E_f$  the formation energy for the spin-polarized calculations,  $E_{min}$  is the minimum energy obtained. The numbers in brackets correspond to the energy minimum for the non-polarized calculations.

It is found that Fe<sub>50</sub>Al<sub>50</sub> retains a magnetic moment of 0.64 $\mu_B$ , even though the phase diagram of this system shows that this alloy is not magnetic at room temperature [12]. The energy for the spin-polarized calculations has a lower value than for the non-polarized ones; however, it is within the error ( $\sim 0.01eV$ ) that can be obtained with this method; therefore, taking the results of these calculations into account we cannot conclude whether this structure is magnetic or not. It is worth mentioning that this is not the first time that theoretical calculations predict a magnetic moment for this structure and composition; most of the literature shows the same theoretical results that go against experiments in this Fe<sub>50</sub>Al<sub>50</sub> [27, 30, 97, 98]. Moruzzi and Marcus [98] seeing that the energy difference was so small used another criteria to determine whether this alloy for this structure and composition was magnetic or not. They calculated the bulk modulus and compared it with the experimental results and they got to the conclusion that this alloy was ferromagnetic. Kulikov et al. [27] noticed that since the energy difference between the ground states was so small one could conclude that the formation of a spin-glass state was possible in a Fe-Al system. Bogner [30] explained this discrepancy between experiment and calculations by stating that the high density of defects, found in real systems, destroys the atomic periodicity, and this lack of periodicity could cause a decrease of the magnetic moment. In contrast to these results Mohn et al. [93] used LDA+U approximation and got a non-magnetic Fe<sub>50</sub>Al<sub>50</sub> stoichiometric alloy.

	Fe <sub>50</sub> Al <sub>50</sub>		Fe <sub>75</sub> Al <sub>25</sub>	
<b>a<sub>exp</sub> (a.u.)</b>	[98][12][99][100][87]	5.309–5.495	[101] [99]	10.945 10.926
<b>a<sub>theo</sub> (a.u.)</b>	[90][91][27][98][101]	5.330–5.398	[99]	10.8
<b>present work (LDA)</b>	5.37		10.65	
<b>present work (P-W)</b>	5.49		11.00	
<b>B<sub>exp</sub> (Gpa)</b>	[100] [27]	152 150		
<b>B<sub>theo</sub> (Gpa)</b>	190–205 [91][102][98][101]			
<b>present work (LDA)</b>	200		176	
<b>present work (P-W)</b>	171		162	
<b>μ<sub>exp</sub> (μ<sub>B</sub>)</b>	[91]	0	[103] μ <sub>Fe1</sub> =1.46	μ <sub>Fe</sub> =2.14
<b>μ<sub>theo</sub> (μ<sub>B</sub>)</b>	[91][98][30]	0.69–0.71	[30] μ <sub>Fe1</sub> =1.9	μ <sub>Fe</sub> =2.25
<b>present work (LDA)</b>	0.64		μ <sub>Fe1</sub> =1.63	μ <sub>Fe</sub> =2.23
<b>present work (P-W)</b>	0.76		μ <sub>Fe1</sub> =2.05	μ <sub>Fe</sub> =2.48
<b>E<sub>cohe<sub>exp</sub></sub> (eV)</b>	[100]	-3.58		
<b>E<sub>cohe<sub>theo</sub></sub> (eV)</b>	[91] [101]	7.66 -5.91		
<b>present work</b>	-5.90		-7.62	
<b>E<sub>f<sub>exp</sub></sub> (eV)</b>	[104] [105]	-0.26 -0.33		
<b>E<sub>f<sub>theo</sub></sub> (eV)</b>	[91][94][88]	-0.32 – -0.51	[27]	-0.22
<b>present work</b>	-0.46		-0.25	

Table II. Comparison of the obtained results with previous experimental and theoretical results.

Figure 17b shows the variation of the magnetic moment versus the lattice parameter in the B2 structure of Fe<sub>50</sub>Al<sub>50</sub>. In this structure 8 Al atoms surround the Fe atoms and there is a charge transfer between Al and Fe atoms, which makes the distribution of the density of states change with lattice parameter. Next to the equilibrium lattice-parameter there is a jump (from a low to a high moment state) of the mean magnetic moment per iron atom that goes from zero to around 0.6μ<sub>B</sub>. This phenomenon can be explained by taking into account the DOS (see Fig. 18) and the difference between the majority- and minority-spin sub-bands.

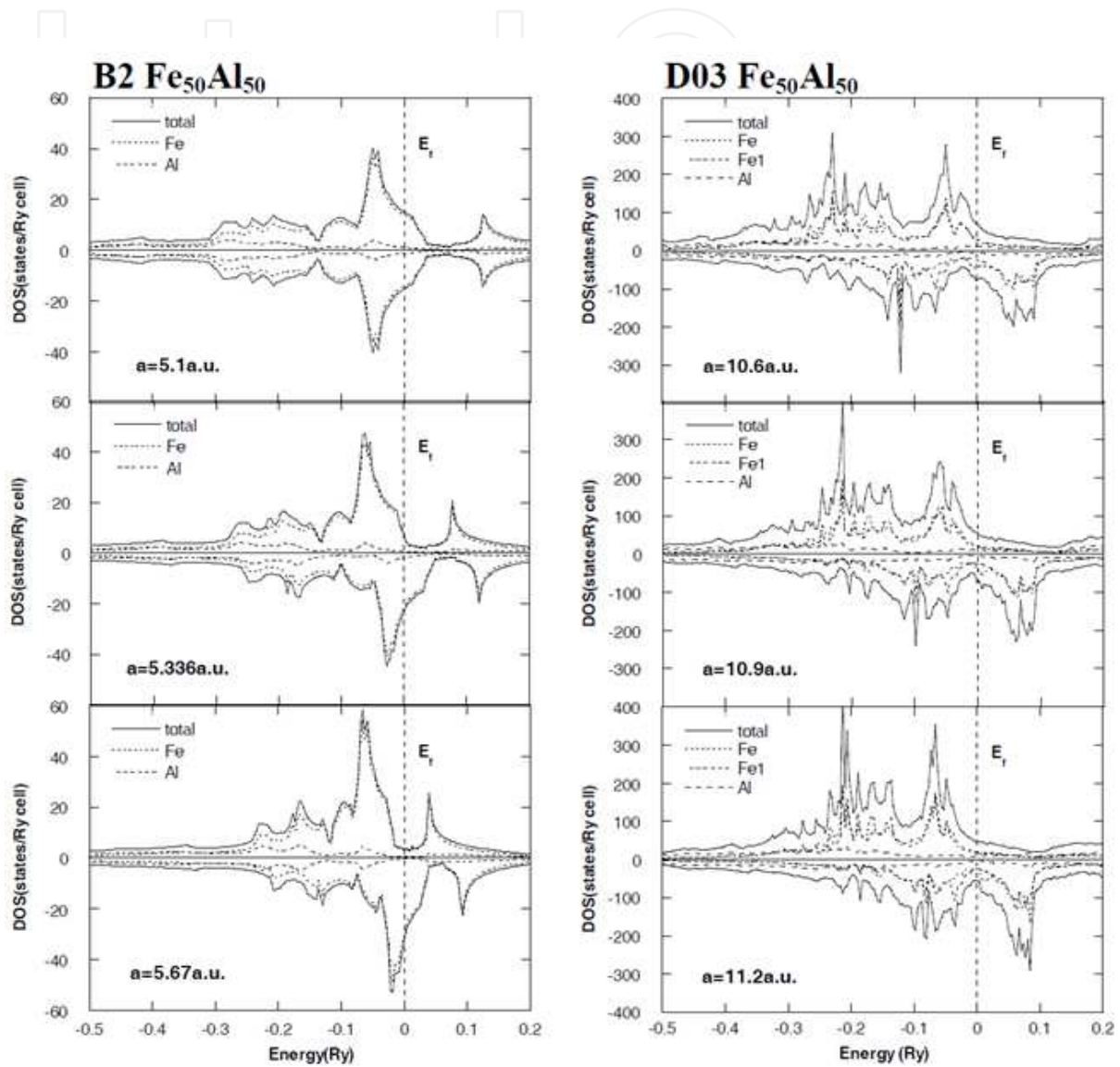


Fig. 18. Density of states calculated for three different lattice parameters of B2 and D03 structures corresponding to  $\text{Fe}_{50}\text{Al}_{50}$  composition. Figure taken from reference [28].

The hybridization causes a charge transfer between the majority- and minority-spin subbands. This decreases the difference between the number of occupied states and consequently weakens the magnetism of the alloy.

If we take a closer look at the density of states versus energy (see Fig. 18), for this structure and this composition, the minority- and majority-spin sub-bands are very similar- they show two peaks separated by a large gap. For small lattice parameters both sub-bands are identical in shape and occupation and the main peak is not completely full. However, as the lattice parameter increases, owing to the decrease of hybridization, there is a charge transfer from the minority to the majority-spin sub-band, that makes the peak of this last band fill up and the one corresponding to the minority-spin sub-band empty. Therefore a magnetic moment appears.

For the D03 structure and  $\text{Fe}_{50}\text{Al}_{50}$  composition a larger difference between the non-magnetic and magnetic states is obtained and we can state that for this structure and this composition the alloy is magnetic with an average magnetic moment of  $1.71\mu_{\text{B}}$  (see Table I). The minimum of the total energy is a little bit higher than the one obtained for the B2 structure, which is in agreement with the fact that B2 is the equilibrium phase for this composition.

The behavior of the average magnetic moment with varying the lattice parameter is completely different from the one shown previously (see Fig. 17, D03 structure). It increases monotonically from  $0.5\mu_{\text{B}}$  to  $1.9\mu_{\text{B}}$ , without showing any jump with the increase of the lattice parameter. There are two non-equivalent Fe atoms, which have the same next-nearest-neighborhood (4 Al and 4 Fe atoms) and show also a continuous increase of the magnetic moment with the lattice parameter. The magnetic moment of one of the Fe atoms in the equilibrium lattice-parameter is 2 % larger than for the other. This small difference could be attributed to the 2<sup>nd</sup> nearest neighbor environment; the one with the larger magnetic moment has 2 Fe and 4 Al atoms as 2<sup>nd</sup> nearest neighbors while the other has only Al atoms as 2<sup>nd</sup> nearest neighbors.

This behavior can be explained by taking into account the density of states, which is completely different from the one shown before. In this case, the majority-spin sub-band is almost full even for small lattice parameters and the Fermi energy is in the gap of the minority sub-band. As in the previous case, the lattice-parameter change causes a change in the hybridization of the sp-Al and d-Fe majority- and minority-spin sub-bands that induces a charge transfer between the minority-spin sub-band and the majority-spin sub-band that makes the magnetic moment increase with lattice parameter. However, the changes induced in the magnetic moment will be small because of the majority-spin sub-band is almost full even for small lattice parameters. (see Fig. 18).

For the B32 structure and  $\text{Fe}_{50}\text{Al}_{50}$  the difference between the energy of the polarized and not polarized calculations tells us that this structure is magnetic for this composition (see Table I) with a mean magnetic moment that increases monotonically with the lattice parameter. The very low bulk modulus (44 Gpa) is related to the fact that this structure does not exist for the studied composition, and it indicates that the actual compositions with this structure are far from  $\text{Fe}_{50}\text{Al}_{50}$ . This is consistent with the phase diagram where this phase does not exist for this composition.

The results for  $\text{Fe}_{75}\text{Al}_{25}$  are summarized in Table I. We can say that the D03 structure has the lowest energy in agreement with the phase diagram that shows this phase for this composition.

For higher Fe contents, two different concentrations in the Fe-richest side of the phase diagram were chosen and two cells that fulfill the DO3 and B32 structures conditions were built (see Table I). The calculations indicate that the stable structures are the stoichiometric ones, i.e.  $\text{Fe}_{75}\text{Al}_{25}$  for the DO3 and  $\text{Fe}_{50}\text{Al}_{50}$  for the B2 structure and this is in agreement with the phase diagram [106]. On the other hand, it has been shown that the bulk modulus for the B32 ( $\text{Fe}_{50}\text{Al}_{50}$ ) structure is very low, but as the concentration of Fe grows, so does the bulk modulus, and its values are closer to the values measured in the phases corresponding to this composition. This is a clear indication that the B32 structure can exist only for high Fe content compositions far from  $\text{Fe}_{50}\text{Al}_{50}$  composition.

Summarizing, it can be concluded from the analyzed structures that in the previous composition the density of states has a really large importance for the behavior of the magnetic moment. When the majority subband is completely full the magnetic moment is high. This is due to the hybridization that induces intraband charge transfer in these alloys. This is also the reason why abrupt DOS changes with lattice parameter cause magnetic moment jump from low to high moment state.

It is interesting to notice that the behavior of the non-equivalent Fe positions with the lattice parameter is quite similar when they have similar environment, independently of the structure under which the calculations are performed.

The calculations indicate that the number of Fe atoms in the nearest neighborhood of one Fe atom, which are needed to cause an abrupt jump of its magnetic moment (with the variation of the lattice parameter) increases as the Fe-content in the alloy increases. In addition, table I indicates that the equilibrium lattice-parameter decreases with the increase of Fe content in the alloy. As expected, the magnetic moment increases with Fe content.

## 5.2 Disordered structure (A2)

As we have seen in the previous section most of the theoretical work done to study the reinforcement of magnetism in these alloys by disordering has been performed assuming point defects [90, 96, 107] and antiphase boundaries [27]. Nevertheless, several articles have studied, by self-consistent methods, the disordered structures for compositions near the equiatomic B2 one using the Coherent Potential Approximation (CPA) [29, 97]. Kulikov et al. [27] found magnetism in the range of disordered alloys studied, but contrary to the experimental results, they found a decrease of lattice parameter with disordering in all the studied composition range.

Taking into account that X-ray diffraction of severe cold-deformed (mechanically milled) FeAl alloys shows diffraction peaks corresponding to the A2 structure [108, 109], and that this structure also appears in samples prepared by rapid quenching from the melt, we have simulated the disorder in FeAl alloys by means of the A2 structure. On the other hand, the magnetic properties depend strongly on the local environment, which at the same time depends on the chosen cell. Therefore, in order to make a good approximation, the average of seven different A2 supercells for  $\text{Fe}_{50}\text{Al}_{50}$  composition and seven different A2 supercells for  $\text{Fe}_{75}\text{Al}_{25}$  composition have been used to compare theoretical and experimental results.

The spin-polarized calculations have a lower energy than the non-polarized ones (not shown) and therefore, we can conclude that for these structures and compositions these alloys are magnetic in all the different cells built, independently of the Fe content ( $\text{Fe}_{50}\text{Al}_{50}$  or  $\text{Fe}_{75}\text{Al}_{25}$ ). Table III shows that the equilibrium lattice parameter decreases with the increasing Fe content in the alloy. The values of the lattice parameter obtained (see Tables II and III) underestimate by less than 3% the experimental value obtained by Frommeyer et al. [101] in deformed or ball milled samples of  $\text{Fe}_{70}\text{Al}_{30}$  that possess the A2 structure. It is worth mentioning that this underestimate is of the same order as the one found between the  $\text{Fe}_{75}\text{Al}_{25}$ -D03 theoretical and experimental values.

Composition	Structure	a (a.u.)	$\mu_{\text{Fe}}(\mu_{\text{B}})$	$E_{\text{pol}}^{\text{min}}(\text{Ry})$
$\text{Fe}_{50}\text{Al}_{50}$	B2	10.74	0.64	-275.1255
	A2	10.96	1.75	-275.1210
$\text{Fe}_{75}\text{Al}_{25}$	D03	10.65	1.86	-300.3854
	A2	10.72	2.01	-300.3842

Table III. Comparison of the results between ordered and disordered structures.

Table III clearly shows that the mean magnetic moment corresponding to the structure with  $\text{Fe}_{75}\text{Al}_{25}$  composition is larger than the one for  $\text{Fe}_{50}\text{Al}_{50}$  composition. It also indicates that the calculated energy minimum in the disordered structures (A2) is above the ones corresponding to the ordered phases. This is in agreement with the fact that in the calculated ranges of compositions the stable structures are the ordered ones. For  $\text{Fe}_{50}\text{Al}_{50}$  composition, the B2 structure has the lowest energy and this is the structure that appears in the phase diagram for this composition.

The equilibrium lattice-parameters for the calculated A2 structures are larger than the corresponding ordered (B2 and D03) ones. This is again in good agreement with X-ray diffraction observations after severe deformation of alloys of similar composition, where the lattice parameter increases with deformation of the alloy. However, it disagrees with the calculations performed under the KKR-CPA approach [27]. Moreover, it must be mentioned that the theoretical increase of the lattice parameter between the A2 and the D03 structures of  $\text{Fe}_{75}\text{Al}_{25}$  is 0.75%, and is in very good agreement with the experimental increase after deformation of about 0.7% found for  $\text{Fe}_{70}\text{Al}_{30}$  [101; see section 3]. In the case of  $\text{Fe}_{50}\text{Al}_{50}$  the lattice parameter increases by 2% due to disorder. That is to say, the results obtained are in good agreement with the experimental ones.

Table III shows that the magnetic moment per iron atom increases with increasing disorder. This is specially pronounced in the case of  $\text{Fe}_{50}\text{Al}_{50}$  (B2), where the magnetic moment increases more than  $1 \mu_{\text{B}}$  after disordering. These theoretical results are in agreement with the experimentally observed increase of the magnetism in deformed or ball-milled alloys [13, 14, 84; see section 3], which, as previously cited, also show an increase in the lattice parameter with any type of deformation.

Figure 19 shows the density of states with respect to the energy for an ordered and a disordered structure of  $\text{Fe}_{50}\text{Al}_{50}$  composition. Owing to the lower lattice parameter for the B2 structure, the hybridization is larger than for the disordered structure and therefore the difference between the two bands is larger in the disordered case, which causes the magnetic moment to be higher. In addition to this, the nearest neighbor configuration of each iron atom (in the disordered structure not every iron atom is surrounded by 8 Al atoms, as it happens in the B2  $\text{Fe}_{50}\text{Al}_{50}$ ) favors a larger magnetic moment.

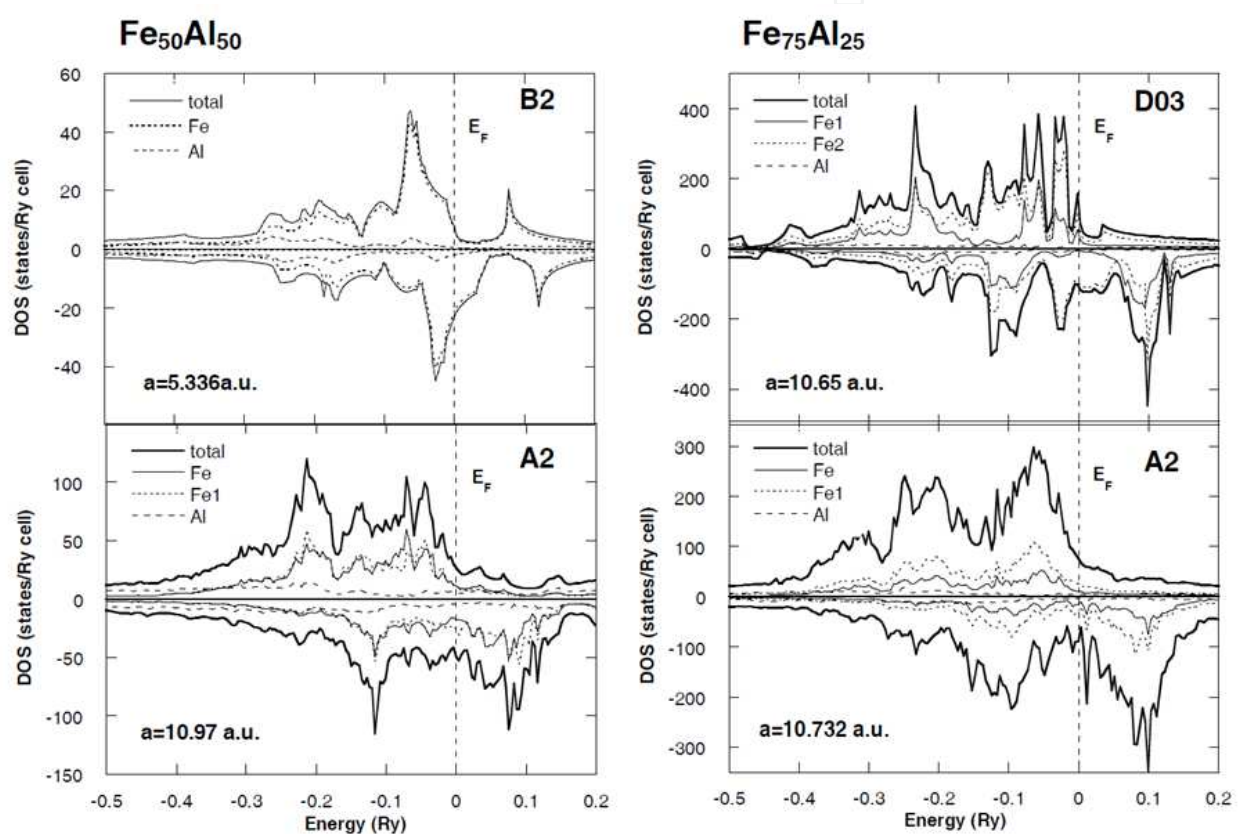


Fig. 19. Comparison of the DOS of ordered and disordered structures at the equilibrium volume for two different compositions.

Hernando et al. [14] found that an important contribution to the magnetism of these alloys comes from changes in the lattice parameter induced by the order-disorder transition. This contribution is linked to modifications in the electronic band structure induced by volume changes. In the present work, it was clearly shown, through the study of the lattice-parameter dependence of the magnetic moment, that this effect is important in a variety of structures and compositions that were studied. However, our results indicate that the disorder has also a large contribution. In the following table we have calculated the weight of each contribution for two compositions (see Table IV),

Composition	Structure	Weight (%)	
		Volume increase	Order-Disorder
Fe <sub>50</sub> Al <sub>50</sub>	B2	13	87
Fe <sub>75</sub> Al <sub>25</sub>	D03	45.5	54.5

Table IV. Average value (of the different ways to obtain theoretically the contributions, see [68]) of the weight of each of the contributions to the magnetic moment increase in the disordering process for two different concentrations.

It is interesting to notice that the values presented in table IV match the experimental values obtained by the XMCD experiments presented in section 3.1, where in the case of the disordered Fe<sub>60</sub>Al<sub>40</sub> alloy the volume change contribution amounted to 35±5%.

Summarizing, the comparison between calculations performed in ordered and disordered structures of the same composition indicates that the disorder makes both the lattice parameter and the magnetism increase in comparison to the ordered structures. Indeed, the lattice parameter increase with disorder for Fe<sub>50</sub>Al<sub>50</sub> and Fe<sub>75</sub>Al<sub>25</sub> alloys is in good agreement with experimental results. The contribution of disorder to the magnetism of these alloys depends on the Fe content of the alloy. The disorder gives the largest contribution close to the equiatomic FeAl alloy, but in Fe<sub>75</sub>Al<sub>25</sub> alloy its contribution is similar to the one given by the volume change.

## 6. Acknowledgments

We want to acknowledge the financial support from the UPV/EHU, Basque Government and the Spanish Government under Grants No. IT-443-10 and No. MAT2009-14398.

## 7. References

- [1] J.H. Westbrook, R.L. Fleicher, *Intermetallics compounds Vol. I: Principles, Vol. 2: Practice*, New York, Wiley (1995) 4
- [2] G. Sauthoff, *Intermetallics*, Werthaeim:VHC (1995)
- [3] J.C. Wang, D.G. Liu, M.X. Chen, X.X. Cai, *Scripta Metallurgica* 25 (1991) 2581
- [4] A. Taylor and R. M. Jones, *J. Phys. Chem. Solids* 6, 16-37 (1958)
- [5] A. Arrot and H. Sato, *Phys. Rev.* 114, 1420 (1959).
- [6] P. Huffman and R. M. Fisher, *J. Appl. Phys.* 38, 735 (1967)
- [7] I. Vincze, *phys. Stat. Sol. (a)* 7 (1971) K43
- [8] M.J. Besnus, A. Herr and A.J.P. Meyer, *J. Phys. F: Metal Phys.* 5 2138 (1975)
- [9] D.A. Eelman, J.R. Dahn, G.R. Macklay, R.A. Dunlap, *J. Alloys and Compounds* 266 (1998) 1
- [10] P.A. Beck, *Metallurgical Transactions (AIME)* 2, 2015 (1971).
- [11] L. Hedin, B.I. Lundqvist, *J. Phys. C4* (1971) 2064
- [12] R. Kuentzler, *J. Physique* 44 (1983)
- [13] I. Turek, V. Drchal, J. Kudrnovský, M.Sov, P. Weinberger, *Electronic structure of disordered alloys, surfaces and interfaces* Kluwer Academic Publishers, Boston-London-Dordrecht (1997) p. 15

- [14] A. Hernando, X. Amils, J. Nogués, S. Suriñach, M. D. Baró, and M. R. Ibarra, *Phys. Rev. B* 58, R11864 (1998)
- [15] Iron binary phase diagrams. Berlin: Springer-Verlag, 1982.
- [16] R. C. Hall, *J. Appl. Phys.* 30, 816 (1959)
- [17] A.E. Clark, J.B. Restorff, M. Wun-Fogle, D. Wu and T.A. Lograsso, *J. Appl. Phys.*, 103, 07B310 (2008)
- [18] Z.H. Liu, G.D. Liu, M. Zhang, G.H. Wu, F.B. Meng, H.Y. Liu, L.Q. Yan, J.P. Qu and Y.X. Li. *Appl. Phys. Lett.*, 85, 1751 (2004)
- [19] C. Jiang, X.X. Gao, J. Zhu and S.Z. Zhou. *J. Appl. Phys.*, 99, 023903 (2006)
- [20] R. Sato Turtelli, G. Vlášak, F. Kubel, N. Mehmood, M. Kriegisch, R. Grössinger, and H. Sassik, *IEEE Trans. Magn.*, 46, 483 (2010)
- [21] N. Mehmood, R. Sato Turtelli, R. Grössinger, M. Kriegisch, *J. Magn. Magn. Mater.* 322, 1609 (2010).
- [22] P. Shukla, M. Wortis, *Phys. Rev. B* 21 (1980) 159
- [23] B.D. Cullity, *Introduction to Magnetic Materials*, Addison-Wesley Publishing Company (1972) 134
- [24] J.S. Kouvel, *J. Appl. Phys.* 30 313S (1959)
- [25] J.S. Kouvel, *Magnetism and Metallurgy*, Vol. 2, p. 523. Academic Press. 1969
- [26] Y. Yang, I. Baker and P. Martin, *Phil. Mag. B* 79, 449 (1999)
- [27] N. I. Kulikov, A.V. Postnikov, G. Borstel and J. Braun, *Phys. Rev. B* 59, 6824 (1999)
- [28] E. Apiñaniz, F. Plazaola, J.S. Garitaonandia, *Eur. Phys. J. B* 31 (2003) 167.
- [29] S.K. Bose, V. Drchal, J. Kudrnovsky, O. Jepsen and O.K. Andersen, *Phys. Rev. B* 55, 8184 (1997).
- [30] J. Bogner, W. Steiner, M. Rissner, P. Mohn, P. Blaha, K. Schwarz, R. Krachler and H. Ipsi, *Phys. Rev. B* 58, 22 (1998)
- [31] H. Gengnagel, M. J. Besnus, and H. Danan, *Phys. Status Solidi A* 13, 499 (1972)
- [32] D. Martin Rodriguez, F. Plazaola, J.S. Garitaonandia, J.A. Jimenez, E. Apiñaniz, *Intermetallics* 24, 38 (2012)
- [33] D. S. Schmool, E. Araujo, M. M. Amado, M. Alegria Feio, D. Martin Rodriguez, J. S. Garitaonandia and F. Plazaola, *J. Magn. Magn. Mater.* 272-276, 1342 (2004).
- [34] H. Sato and A. Arrot, *Phys. Rev.* 114, 1427 (1959).
- [35] S.J. Pickart and R. Nathans, *Phys. Rev. B* 123, 1163 (1961).
- [36] J.P. Perrier, B. Tissier and R. Tournier, *Phys. Rev. Lett.* 24 313 (1970).
- [37] R.D. Shull, H. Okamoto and P.A. Bech, *Solid State Commun.* 20 863 (1976).
- [38] K. Motoya, S.M. Shapiro and Y. Muraoka, *Phys. Rev. B* 28, 6183 (1983).
- [39] G.P. Huffman, in *Amorphous Magnetism*, p. 283. Ed. H.O. Hooper and A.M. de Graaf, (Plenum New York, 1973).
- [40] J. S. Garitaonandia, E. Apiñaniz, F. Plazaola, *Bulletin of the APS* 47, 1, p. 339 (2002)
- [41] S. Mitsuda, H. Yoshizawa and Y. Endoh, *Phys. Rev. B* 45, 9788 (1992)
- [42] P. Böni, S.M. Shapiro and K. Motoya, *Phys. Rev. B* 37, 243 (1988).
- [43] Wei Bao, S. Raymond, S.M. Shapiro, K. Motoya, B. Fåk and R.W. Erwin, *Phys. Rev. Lett.* 82, 4711 (1999)

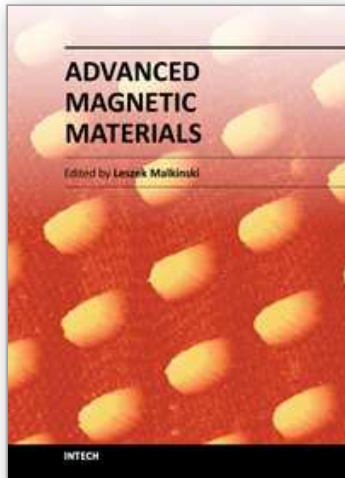
- [44] J.W. Cable, L. David and R.Parra, *Phys. Rev. B* 16, 1132 (1977)
- [45] T.M. Srinivasan, H. Claus, R. Viswanathan, P.A. Beck and D.I. Bardos in *Phase Stability in Metals and Alloys*, p.151. Ed. P.S. Rudman, J. Stringer and R.I. Jaffee (MacGraw-Hill New York, 1967)
- [46] H. Maletta, G. Aeppli and S.M. Shapiro, *Phys. Rev. Lett.* 48, 1490 (1982)
- [47] G. Aeppli, S.M. Shapiro, R.J. Birgeneau and H.S. Chen, *Phys. Rev. B* 25, 4882 (1982)
- [48] E. P. Yelsukov, E. V. Voronina, and V. A. Barinov, *J. Magn. Magn. Mater.* 115, 271 (1992)
- [49] S. Takahashi and Y. Umakoshi, *J. Phys.: Condens. Matter* 2, 4007(1990)
- [50] X. Amils, J. Nogués, S. Suriñach, M. D. Baró, and J. S. Muñoz, *IEEE Trans. Magn.* 34, 1129 (1998)
- [51] R. A. Varin, T. Czujko, J. Bystrzycki, and A. Calla, *Mater. Sci. Eng., A* 329-331, 213 (2002)
- [52] M. Fujii, K. Katuyoshi, K. Wakayama, M. Kawasaki, T. Yoshioka, T. Ishiki, N. Nishio, and M. Shiojiri, *Philos. Mag. A* 79, 2013 (1999)
- [53] W. Hu, T. Kato, and M. Fukumoto, *Mater. Trans., JIM* 44, 2678 (2003)
- [54] X. Amils, J. Nogués, S. Suriñach et al. J. S. Muñoz, *Phys. Rev. B* 63, 52402 (2001)
- [55] D. Negri, A. R. Yavari, and A. Deriu, *Acta Mater.* 47, 4545 (1999)
- [56] L. F. Kiss, D. Kaptás, J. Balogh, L. Bujdosó, T. Kemény, I. Vincze, and J. Gubicza, *Phys. Rev. B* 70, 012408 (2004)
- [57] G. K. Wertheim, V. Jaccarino, J. H. Wernick, and D. N. E. Buchanan, *Phys. Rev. Lett.* 12, 24 (1964)
- [58] P. Shukla and M. Wortis, *Phys. Rev. B* 21, 159 (1980)
- [59] J. A. Plascak, L. E. Zamora, and G. A. Pérez Alcazar, *Phys. Rev. B* 61, 3188 (2000)
- [60] A. Arzhnikov, A. Bagrets, and D. Bagrets, *J. Magn. Magn. Mater.* 153, 195 (1996)
- [61] M. Shiga, *J. Phys. Soc. Jpn.* 50, 2573 (1981)
- [62] M. Shiga, *IEEE Transl. J. Magn. Jpn.* 6, 1039 (1991)
- [63] A. Hernando, J. M. Barandiarán, J. M. Rojo, and J. C. Gómez-Sal, *J. Magn. Magn. Mater.* 174, 181 (1997)
- [64] B. V. Reddy, S. C. Deevi, F. A. Reuse, and S. N. Khanna, *Phys. Rev. B* 64, 132408 (2001)
- [65] A. V. Smirnov, W. A. Shelton, and D. D. Johnson, *Phys. Rev. B* 71, 064408 (2005)
- [66] V. L. Moruzzi, P. M. Marcus, *Phys. Rev. B*, 47, 7878 (1993)
- [67] E. Apiñaniz, F. Plazaola, J. S. Garitaonandia, *J. Non Cryst. Solids* 287, 302 (2001)
- [68] E. Apiñaniz, F. Plazaola et al. *J. Magn. Magn. Mater.* 272, 794 (2004)
- [69] J. Deniszczyk, *Acta Phys. Pol. A* 97, 583 (2000)
- [70] J. Nogués, E. Apiñaniz, J. Sort, M. Amboage, M. d'Astuto, O. Mathon, R. Puzniak, I. Fita, J. S. Garitaonandia, S. Suriñach, J. S. Muñoz, M. D. Baró, F. Plazaola, and F. Baudelet, *Phys. Rev. B* 74, 024407 (2006)
- [71] E. Apiñaniz, F. Plazaola, J. S. Garitaonandia, D. Martin and J.A. Jimenez, *J. Appl. Phys.* 93, 7649 (2003)
- [72] E. Apiñaniz, J.S. Garitaonandia, F. Plazaola, D. Martin, J.A. Jimenez, *Sensors and Actuators A*, 106 76 (2003)

- [73] J. F. Humphreys, in *Materials Science and Technology: A Comprehensive Treatment*, edited by R. W. Cahn *et al.* (VCH, Weinheim 1992), Vol. 15.
- [74] D. Wu, P. R. Munroe and I. Baker, *Phil. Mag.* 83, 295 (2003).
- [75] D. Martin Rodriguez, E. Apinaniz, J. S. Garitaonandia, F. Plazaola, D. S. Schmool and G. Cuello, *J. Magn. Magn. Mater.* 272-276, 1510 (2004)
- [76] D. Martin Rodriguez, E. Apinaniz, F. Plazaola, J. S. Garitaonandia, J. A. Jimenez, D. S. Schmool and G. J. Cuello, *Phys. Rev. B* 71, 212408 (2005).
- [77] S. M. Allen and J. W. Cahn, *Acta Metall.* 24, 425 (1976)
- [78] K. Yamashita, M. Imai, M. Matsuno and A. Sato, *Phil. Mag. A* 78, 285 (1998).
- [79] A. E. Vidoz and L. M. Brown, *Phil. Mag.* 7, 1167 (1962).
- [80] C. T. Chou and P. B. Hirsch, *Phil. Mag. A* 44, 1415 (1981).
- [81] H. Y. Yasuda, R. Jimba and Y. Umakoshi, *Scripta mater.* 48, 589 (2003).
- [82] M. van Schilfgaarde, I. A. Abrikosov and B. Johansson, *Nature* 400, 46 (1999)
- [83] Z. Arnold, J. Kamarad, P. A. Algarabel, B. Garcia-Landa and M. R. Ibarra, *IEEE Trans. Magn.* 30, 619-621 (1994)
- [84] V. L. Moruzzi, A. R. Williams and J. F. Janak, *Phys. Rev. B* 10 (1974) 4856
- [85] C. Müller, H. Wonn, W. Blau, P. Ziesche and V.P. Krivitskii, *Phys. Status Solidi B* 95 (1979) 215
- [86] C. Müller and P. Ziesche, *Phys. Status Solidi B* 114 (1982) 523
- [87] C. Müller, W. Blau and P. Ziesche, *Phys. Status Solidi B* 116 (1983) 561
- [88] J. Zou and C. L. Fu, *Phys. Rev. B* 51 (1995) 4
- [89] J. H. Westbrook and R. L. Fleischer, *Intermetallic Compounds* Wiley Chicester (1994), Vol. 1, p.127
- [90] R. E. Watson and M. Weinert, *Phys. Rev. B* 58 (1998) 5981
- [91] V. Sundararajan, B. R. Sahu, D. G. Kanhere, P. V. Panat and G. P. Das, *J. Phys.: Condens. Matter* 7 (1995) 6019
- [92] B. I. Min, T. Oguchi, H. J. F. Jansen and A. J. Freeman, *J. Magn. Mag. Mat.* 54-57 (1986) 1091
- [93] P. Mohn, C. Persson, P. Blaha, K. Schwarz, P. Novák, H. Eschrig, *Phys. Rev. Letters* 87 (2001) 6401 (edo 196401)
- [94] Y. M. Gu and L. Fritsche, *J. Phys.: Condens. Matter* 4 (1992) 1905
- [95] W. Lin, Jian-hua Xu and A. J. Freeman, *J. Mater. Res.* 7 (1992) 592
- [96] C. L. Fu, *Phys. Rev. B* 52 (1995) 315
- [97] J. Mayer, C. Elsässer and M. Fähnle, *Phys. Stat. Sol.(b)* 191, 283 (1995)
- [98] V. L. Moruzzi and P. M. Marcus, *Phys. Rev. B* 46, 2864 (1993)
- [99] S. Dorfman, V. Liubich, D. Fuks, *Inter. J. Quantum Chem.* 75, 4 (1999)
- [100] F. Schmidt and K. Binder, *J. Phys.: Condens. Matter* 4, 3569-3588 (1992)
- [101] G. Frommeyer, J.A. Jimenez, C. Derder, *Z. Metallkd.* 90, 43 (1999)
- [102] R. Haydock, M.V. You, *Solid State Comm.* 33, 299 (1980)
- [103] R. Nathans, H.T. Pigott, C.G. Shull, *J. Phys. Solids* 6, 38(1958)
- [104] P. Villars, L.D. Calvert, *Pearson's Handbook of Crystallographic Data for Intermetallic Phases*, Vols. 1-3 (Metals Park, OH: American Society for Metals, 1985)
- [105] F.R. de Boer, R. Boom, W.C. Mattens, A.R. Miedema, A.K. Niesen, *Cohesion Metals: Transition Metal Alloys* (North-Holland, Amsterdam, 1988)

- [106] O. Kubaschewski, *Iron Binary Phase Diagrams* (Springer, Berlin, 1986)  
[107] G. Bester, B. Meyer, M. Fähnle, *Phys. Rev. B* 60, No. 21, 14492 (1999)  
[108] B. Fultz, Z. Gao, *Phil. Mag. B* 67, 6 (1993)  
[109] D. Rafaja, *Scripta Mat.* 34, 9 (1996)

IntechOpen

IntechOpen



## **Advanced Magnetic Materials**

Edited by Dr. Leszek Malkinski

ISBN 978-953-51-0637-1

Hard cover, 230 pages

**Publisher** InTech

**Published online** 24, May, 2012

**Published in print edition** May, 2012

This book reports on recent progress in emerging technologies, modern characterization methods, theory and applications of advanced magnetic materials. It covers broad spectrum of topics: technology and characterization of rapidly quenched nanowires for information technology; fabrication and properties of hexagonal ferrite films for microwave communication; surface reconstruction of magnetite for spintronics; synthesis of multiferroic composites for novel biomedical applications, optimization of electroplated inductors for microelectronic devices; theory of magnetism of Fe-Al alloys; and two advanced analytical approaches for modeling of magnetic materials using Everett integral and the inverse problem approach. This book is addressed to a diverse group of readers with general background in physics or materials science, but it can also benefit specialists in the field of magnetic materials.

### **How to reference**

In order to correctly reference this scholarly work, feel free to copy and paste the following:

F. Plazaola, E. Apiñaniz, D. Martin Rodriguez, E. Legarra and J. S. Garitaonandia (2012). Fe-Al Alloys' Magnetism, Advanced Magnetic Materials, Dr. Leszek Malkinski (Ed.), ISBN: 978-953-51-0637-1, InTech, Available from: <http://www.intechopen.com/books/advanced-magnetic-materials/fe-al-alloys-magnetism>

**INTECH**  
open science | open minds

### **InTech Europe**

University Campus STeP Ri  
Slavka Krautzeka 83/A  
51000 Rijeka, Croatia  
Phone: +385 (51) 770 447  
Fax: +385 (51) 686 166  
[www.intechopen.com](http://www.intechopen.com)

### **InTech China**

Unit 405, Office Block, Hotel Equatorial Shanghai  
No.65, Yan An Road (West), Shanghai, 200040, China  
中国上海市延安西路65号上海国际贵都大饭店办公楼405单元  
Phone: +86-21-62489820  
Fax: +86-21-62489821

© 2012 The Author(s). Licensee IntechOpen. This is an open access article distributed under the terms of the [Creative Commons Attribution 3.0 License](#), which permits unrestricted use, distribution, and reproduction in any medium, provided the original work is properly cited.

IntechOpen

IntechOpen